The role of tumor endothelial marker 1 in lung metastasis

Dragičević, Dorian

University of Zagreb
Faculty of Science
Department of Biology

Dorian Dragičević

The role of tumor endothelial marker 1 in lung metastasis

Master thesis

Zagreb, 2022.

Sveučilište u Zagrebu
Prirodoslovno-matematički fakultet
Biološki odsjek

Dorian Dragičević

Uloga tumorskog endotelnog markera 1 u metastaziranju pluća

Diplomski rad

Zagreb, 2022.

This thesis was conducted at the Department of Pharmacology, Max Planck Institute for Heart and Lung Research, Bad Nauheim, Germany under the supervision of Prof. Dr. Stefan Offermanns. The thesis has been submitted for evaluation to the Department of Biology, Faculty of Science, University of Zagreb, Zagreb, Croatia in order to acquire the academic title of MSc in Molecular Biology.

ACKNOWLEDGEMENTS

I would like to thank Prof. Dr. Stefan Offermanns for giving me an opportunity to be part of an amazing scientific community and work at the Max Planck Institute for Heart and Lung Research in Bad Nauheim, Germany for six months. I would also like to express my gratitude to every single member of the lab that helped me feel included and welcomed during my stay, especially PhD student Kenneth Anthony Roquid for his support, guidance, and commitment. I am grateful for their involvement and advice during the course of my work.

I would like to thank Assoc. Prof. Dr. Petra Korać for her help and commitment.

I would also like to thank all of my friends and colleagues for their help and support that kept me motivated, making my student years an enjoyable and memorable experience.

Finally, I would like to express my highest appreciation to my family for always being there for me and supporting me.

BASIC DOCUMENTATION CARD

University of Zagreb
Faculty of Science
Department of Biology

Master thesis

The role of tumor endothelial marker 1 in lung metastasis

Dorian Dragičević

Rooseveltov trg 6, 10000 Zagreb, Croatia

Cancer relapse is driven by dormant tumor cells that are able to reactivate after perturbations in the microenvironmental niche. Endothelium-derived protein multimerin 2 (MMRN2) is hypothesized to induce tumor reawakening through the interaction with tumor endothelial marker 1 (TEM1). The main objective of this study was to assess the MMRN2-TEM1 axis in reactivation and proliferation of B16F10 melanoma and E0771 breast cancer cells, and elucidate function of TEM1 in lung metastasis. The MMRN2-TEM1 axis, induced by a co-culture system comprised of endothelial cells and tumor cells, has demonstrated to stimulate phosphorylation of ERK1/2. Individual addition of PDGFB and MMRN2 fragments to dormant tumor cells caused their reactivation, conceivably through the TEM1-PDGFRB pathway. *In vivo* results have shown that absence of TEM1 does not influence primary tumor growth nor extravasation, but reduces macrometastasis formation in both intravenous and resection models of lung metastasis. These *in vivo* results suggest that TEM1 could be implicated in tumor mass dormancy. Computational models have shown significant correlation of TEM1 and PDGFRB as a prediction marker of low survival rates and higher relapse in various tumor types. Therefore, this study presents a pioneering research in defining the MMRN2-TEM1 reactivation axis as a potential target for state-of-the-art, personalized therapies intended for patients in remission.

Keywords: tumor dormancy, tumor reactivation, perivascular niche, multimerin 2, melanoma, breast cancer
(59 pages, 16 figures, 67 references, original in: English)
Thesis is deposited in Central Biological Library.

Mentor: Prof. Stefan Offermanns, PhD
Co-mentor: Assoc. Prof. Petra Korać, PhD

Reviewers:
Assoc. Prof. Petra Korać, PhD
Assoc. Prof. Inga Urlić, PhD
Prof. Biljana Balen, PhD
Assoc. Prof. Petra Peharec Štefanić, PhD

Thesis accepted: September 8, 2022

TEMELJNA DOKUMENTACIJSKA KARTICA

Sveučilište u Zagrebu
Prirodoslovno-matematički fakultet
Biološki odsjek Diplomski rad

Uloga tumorskog endotelnog markera 1 u metastaziranju pluća

Dorian Dragičević

Rooseveltov trg 6, 10000 Zagreb, Hrvatska

Ponovnu pojavu tumora uzrokuju dormantne tumorske stanice koje su sposobne reaktivirati se uslijed promjena u mikrookolišnoj niši. Za endotelni protein multimerin 2 (MMRN2) se pretpostavlja da inducira nastanak tumora, stupanjem u interakciju s tumorskim endotelnim markerom 1 (TEM1). Glavni cilj ovoga rada bio je procijeniti ulogu osi MMRN2-TEM1 u reaktivaciji i proliferaciji stanica melanoma B16F10 i stanica tumora dojke E0771 te razjasniti funkciju proteina TEM1 u metastaziranju pluća. Pokazano je da os MMRN2-TEM1, inducirana kokulturom endotelnih stanica i tumorskih stanica, može stimulirati fosforilaciju proteina ERK1/2. Pojedinačni dodaci proteina PDGFRB i fragmenata MMRN2 dormantnim tumorskim stanicama uzrokovali su njihovu reaktivaciju, potencijalno signalnim putem TEM1-PDGFRB. Rezultati *in vivo* su pokazali da nedostatak proteina TEM1 ne utječe na rast primarnog tumora ni proces ekstravazacije, ali smanjuje formaciju makrometastaza u intravenoznom i resekcijskom modelu plućnog metastaziranja. Navedeni rezultati *in vivo* upućuju na to da protein TEM1 može biti uključen u regulaciju tumorske mase tijekom dormancije. Računalni modeli su ukazali na značajnu povezanost proteina TEM1 i proteina PDGFRB kao predikcijskog markera smanjenog preživljenja i češće ponovne pojave tumora kod brojnih tipova tumora. Ovaj rad predstavlja inicijalno istraživanje u definiranju reaktivacijske osi MMRN2-TEM1, kao potencijalne mete suvremenih, personaliziranih terapija namijenjenih pacijentima u remisiji.

Ključne riječi: dormancija tumora, reaktivacija tumora, perivaskularna niša, multimerin 2, melanom, tumor dojke
(59 stranica, 16 slika, 67 literaturnih navoda, jezik izvornika: engleski)
Rad je pohranjen u Središnjoj biološkoj knjižnici

Mentor: Prof. dr. sc. Stefan Offermanns
Komentor: Izv. prof. dr. sc. Petra Korać

Ocjenitelji:
Izv. prof. dr. sc. Petra Korać
Izv. prof. dr. sc. Inga Urlić
Prof. dr. sc. Biljana Balen
Izv. prof. dr. sc. Petra Peharec Štefanić

Rad prihvaćen: 8.8.2022.

TABLE OF CONTENTS

LIST OF ABBREVIATIONS

Abbreviation	Definition
7-AAD	7-Aminoactinomicin D
BM	Bone marrow
BMP	Bone morphogenetic protein
C1q	Complement component 1q
CC	Coiled-coil
CD93	Cluster of differentiation 93
CDK	Cyclin-dependent kinase
CLEC14A	C-type lectin domain containing 14A
COL17A1	Collagen type XVII alpha 1 chain
COL3A1	Collagen type III alpha 1 chain
CTC	Circulating tumor cell
CTFR	CellTrace Far Red
CTLD	C-type lectin domain
CTY	CellTrace Yellow
CXCL12	C-X-C motif chemokine ligand 12
DTC	Disseminated tumor cell
EC	Endothelial cell
ECM	Extracellular matrix
EdU	5-ethynyl-2'-deoxyuridine
EMILIN	Elastin microfibril interfacer
EMT	Epithelial-mesenchymal transition
ER	Estrogen receptor
ERK1/2	Extracellular signal-regulated kinase 1/2
FACS	Fluorescence-activated cell sorting
FAK	Focal adhesion kinase
FGF	Fibroblast growth factor
FUCCI	Fluorescent ubiquitination-based cell cycle indicator
GAPDH	Glyceraldehyde-3-phosphate dehydrogenase

GFP	Green fluorescent protein
HEK293 cell	Human embryonic kidney 293 cell
HER2	Human epidermal growth factor receptor 2
HIF	Hypoxia-inducible factor
HUVEC	Human umbilical vein endothelial cell
i.n.	Intranasal
i.v.	Intravenous
IL	Interleukin
INFγ	Interferon gamma
IVIS	*In vivo* imaging system
KD	Knockdown
KO	Knockout
KPC	Kip1 (p27) ubiquitination-promoting complex
L1CAM	L1 cell adhesion molecule
LSC	Leukemic stem cell
Mac-2BP	Mac-2-binding protein
MAPK	Mitogen-activated protein kinase
MDA-MB-231 cell	M.D. Anderson-Metastatic breast 231 cell
miR-126	microRNA-126
MLCK	Myosin light-chain kinase
MLEC	Mouse lung endothelial cell
MMP	Matrix metalloproteinase
MMRN2	Multimerin 2
MSC	Mesenchymal stem cell
NET	Neutrophil extracellular DNA trap
NK cell	Natural killer cell
NRF2F1	Nuclear receptor subfamily 2 group F member 1
PDGF	Platelet-derived growth factor
PDGFR	Platelet-derived growth factor receptor
PD-L1	Programmed death ligand 1
PDZ	Post synaptic density protein (PSD95), Drosophila disc large tumor suppressor (Dlg1), and zonula occludens-1 protein (zo-1)

PI3K	Phosphoinositide 3-kinase
POSTN	Periostin
PR	Progesterone receptor
s.c.	Subcutaneous
SCF	Skp, Cullin, F-box containing complex
Skp2	S-phase kinase-associated protein 2
TC	Tumor cell
TEM1	Tumor endothelial marker 1
TGFβ	Tumor growth factor beta
TNF	Tumor necrosis factor
TSP1	Thrombospondin 1
VEGF	Vascular endothelial growth factor
VEGFR	Vascular endothelial growth factor receptor
vWF	von Willebrand factor
YAP	Yes-associated protein

1. INTRODUCTION

Tumor metastasis is defined as a highly coordinated multi-step process in which tumor cells from the primary site disseminate to initiate new tumors in distant organs (Gomis & Gawrzak, 2017; Neophytou et al., 2019). As these secondary niches are often unfavorable for these disseminated tumor cells (DTCs) to thrive, they initially become dormant after successful extravasation (Ghajar et al., 2013; Osisami & Keller, 2013). Recently, it has been shown that the lung endothelium specifically instructs extravasated DTCs to become dormant – and that metastatic dormancy almost always preceded DTC reactivation and colonization (Ghajar, 2015; Ghajar et al., 2013; Phan & Croucher, 2020; Risson et al., 2020). Cell intrinsic driver mutations and microenvironment-derived external cues are causative for these DTCs to escape dormancy (Fares et al., 2020; Gomis & Gawrzak, 2017; Phan & Croucher, 2020; Summers et al., 2020). Although the events that are required for these DTCs to form secondary tumors are becoming more established, a lack of druggable dormancy and reactivation factors necessitates more screening and mechanistic studies.

Metastatic dormancy has been hypothesized to be recapitulated in cancer relapse after treatment (Damen et al., 2021; Gomis & Gawrzak, 2017; S. Y. Park & Nam, 2020). Surviving DTCs after treatment are found to be in a dormant state and, in a likewise manner with metastatic dormancy, are localized near endothelial cells. These findings further suggest the indispensable role of the endothelium in tumor cell dormancy in terms of metastasis formation, therapy resistance, and cancer relapse (Ghajar, 2015; Ghajar et al., 2013; Risson et al., 2020). It has been recently shown that multimerin 2 (MMRN2), an endothelial-specific extracellular matrix protein (ECM), inhibited tumor cell dormancy, both *in vitro* and *in vivo*, using MMRN2 knockdown of primary endothelial cells in co-culture experiments and lung metastasis experiments in MMRN2 endothelial cell-specific knockout mouse lines, respectively (Unpublished). As MMRN2 is seen to be ubiquitously expressed in the endothelium, regardless of the presence of tumors, it was hypothesized that the reactivation of tumor cells depended more on the presence of the MMRN2 receptor, tumor endothelial marker 1 (TEM1) – a gene found to be upregulated in metastatic tumor clones in comparison to the dormant ones (Khan et al., 2017; Lorenzon et al., 2012; Tomkowicz et al., 2010; Valdez et al., 2012; Figure 1).

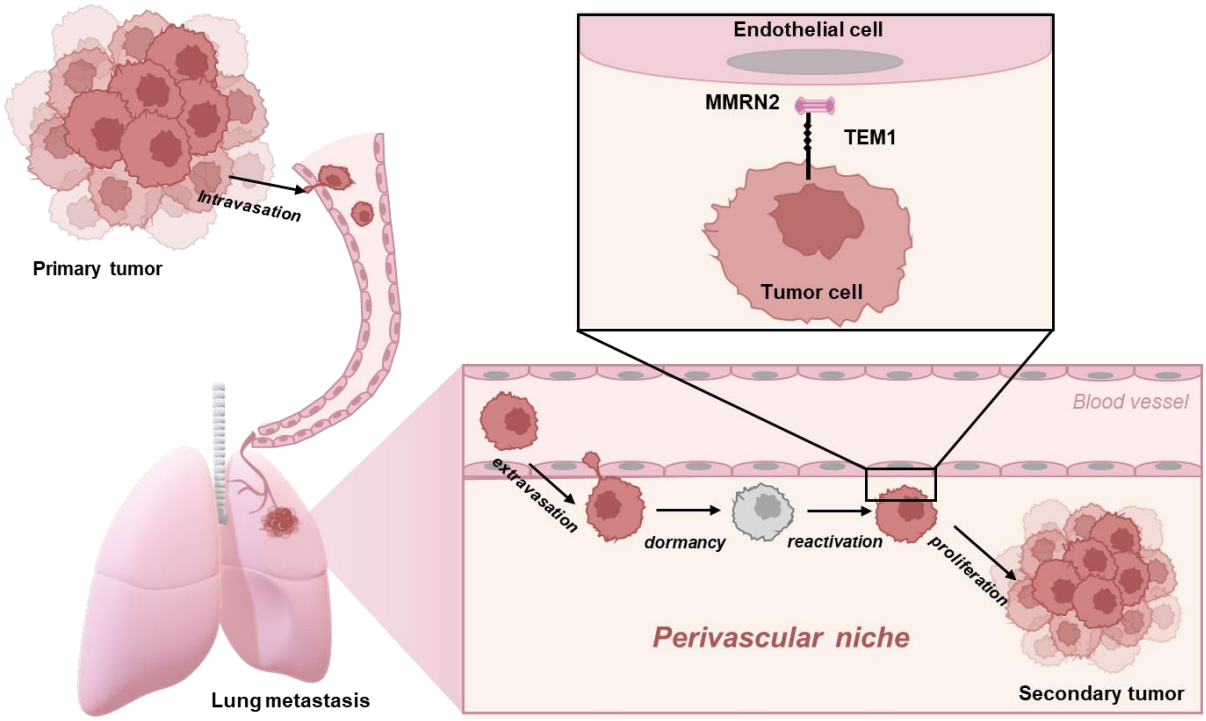

Figure 1. Lung metastatic cascade (Figure created in Microsoft PowerPoint).

Invasive primary tumor cells intravasate, circulate through blood vasculature and extravasate in lung perivascular niche. Upon dissemination, tumor cells reside on the endothelium and can enter dormancy for an undefined period of time before reactivation and metastatic colonization. Endothelial cells are able to regulate dormancy initiation and reawakening through extracellular ligands. The interaction between endothelium-derived extracellular protein – multimerin 2 (MMRN2) and upregulated tumor cell receptor – tumor endothelial marker 1 (TEM1) has been implicated in tumor reactivation and proliferation.

1.1. Tumor cell intravasation and dissemination to secondary sites

The dynamic process of metastatic colonization begins with tumor cells intravasating and leaving the primary tumor site (Gomis & Gawrzak, 2017; Páez et al., 2012; Valastyan & Weinberg, 2011; Yadav et al., 2018). There exists a subpopulation of malignant cells that have acquired mutations to upregulate epithelial-mesenchymal transition (EMT) genes – enabling them to invade functional surrounding tissue and thus, be classified as aggressive and unlocalized (Fares et al., 2020; Neophytou et al., 2019; Valastyan & Weinberg, 2011). Metabolic reprogramming via the Warburg effect increases glucose uptake and aerobic glycolysis of these tumor cells to overcome the inaccessibility of oxygen and nutrients brought by a lack and/or absence of blood vessel formation in the core of the primary tumor mass (Naumov et al., 2006). Additionally, depletion of oxygen and nutrient transport to the primary tumor provides microenvironmental change engendering an angiogenic switch that shifts the balance between pro- and anti-angiogenic factors towards the initiation of new vasculatures (Naumov et al., 2006). These new blood and lymphatic vessels inside the primary tumor serve as a transportation system for tumor cells to disseminate to distant sites and create secondary tumors (Neophytou et al., 2019).

Intravasation of primary tumor cells into the circulation, survival of circulating tumor cells (CTCs), and their extravasation to distant organs has been proven to be an extremely inefficient process. It has been suggested that less than 0.01% of CTCs eventually succeed in the formation of secondary tumor growth (Fares et al., 2020; Gomis & Gawrzak, 2017; Valastyan & Weinberg, 2011). Tropism of certain types of tumors to disseminate to specific organs has been explained by the concept of first-pass organ and seed and soil model (Egeblad et al., 2010). The former hypothesis describes more mechanical aspect of metastatic model where tumor specificity to distant organs is based on trapping CTCs in the capillaries of the first organ they encounter after intravasation from the initial tumor site. The latter hypothesis tries to explain many exemptions from the physiological outlook on metastasis, elucidating that metastatic tumor cells disseminate to sites where microenvironment is more favorable. This concept is supported by the paradigm that the primary tumor influences secondary sites via systemic signaling and exosomes to become less hostile – creating a pre-metastatic niche that supports metastatic colonization and survival of malignant cells at distant organs (Egeblad et al., 2010; Fares et al., 2020; Langley & Fidler, 2011; Osisami & Keller, 2013; Valastyan & Weinberg, 2011).

Upon dissemination, tumor cells can exhibit proliferation, cell death, and/or dormancy. Which of these processes will occur primarily depends on the genetic profile of DTCs as well as the variable microenvironmental factors that influence cellular fate (Montagner & Sahai, 2020). Proliferative ability of DTCs upon arrival to the metastatic site is caused by a favorable microenvironment which can promote undisturbed secondary tumor formation. Cell death is usually triggered by the hostile secondary sites that do not provide complementary extracellular factors, nutrients, and/or stimulating molecules that would prime DTCs to the surrounding stroma. Lastly, dormancy refers to the process that can occur either as a tumor mass, where there is an equilibrium between proliferation and cell death, or on a cellular level, where individual cells exhibit specific genetic and metabolic expression profiles complemented by the cell cycle arrest (Montagner & Sahai, 2020; Valastyan & Weinberg, 2011).

1.2. Tumor mass dormancy

The model of tumor mass dormancy primarily describes regulatory mechanisms inhibiting outgrowth of actively dividing micro/macrometastatic lesions at secondary sites. These malignant cells are organized in clusters comprised of actively proliferating cells, but the size of the foci remains unchanged and indolent for an extended period of time since the rates of proliferation and apoptosis are equal (Osisami & Keller, 2013). Consequently, tumor mass dormancy is mainly based on the interaction between proliferative ability of DTCs at metastatic sites and inhibitory constraints that counterbalance their expansion, preventing their further development into clinically detectable metastasis either by mechanisms of insufficient angiogenesis or active immunoregulation (Risson et al., 2020; Yeh & Ramaswamy, 2015). All of the mentioned processes are highly integrated and coordinated by the tumor microenvironment via a complex network of signals that either promote or sustain aggressive growth.

The notion that tumor dormancy is initiated by various stromal signals and that metastasis-initiating cells are required to escape from the effect of organ-specific inhibiting signals has been experimentally proven in many types of cancer (Almog, 2010; Neophytou et al., 2019; Summers et al., 2020).

1.1.1. Angiogenic dormancy

The vast majority of tumors require the activation of angiogenesis – recruitment and sprouting of new blood vessels from the existing vasculature – in order to promote tumor growth. Diffusion of oxygen and nutrients to the malignant cells is limited when a size of 1-2 mm is reached by the tumor mass, causing metabolic deficiencies that prevent its outgrowth (Hanahan & Weinberg, 2011; Holmgren & Folkman, 1995). Microenvironment of these avascular dormant tumors insufficiently supports the nutritional needs of the large number of malignant cells so they exhibit balanced proliferation and apoptosis rates, and remain microscopic in size (Almog, 2010). Inability of these proliferation-competent cells to express or induce pro-angiogenic factors (such as VEGF, PDGF, FGF, and angiopoietin to promote vasculature sprouting) and the presence of dormant tumor cell-derived molecules (such as miR-126) that inhibit recruitment of endothelial cells are some of the key causes of angiogenic dormancy (Páez et al., 2012; Png et al., 2011). Acquiring non-angiogenic tumors with sufficient angiogenic-related mutations and overexpression of pro-angiogenic chemokines is necessary to surpass inhibitory activity of anti-angiogenic factors (such as TSP1, endostatin, vasculostatin, and angiostatin) that eventually lead to fast-proliferating tumors (Gomis & Gawrzak, 2017; Páez et al., 2012). Concurrently, genetic alterations in the main cellular cascade pathways (such as the oncogenic activation of Ras and/or the loss of tumor suppressor activity of p53 or stress-activated kinase p38) has been shown to aid tumor cells in escaping tumor mass dormancy since they upregulate an angiogenic factor VEGFA while repressing thrombospondin 1 (TSP1) – a known anti-angiogenic molecule (Indraccolo et al., 2006a; Indraccolo et al., 2006b; Páez et al., 2012).

1.1.2. Immunologic (immunomediated) dormancy

The role of the immune system in regulating tumorigenesis has been primarily focused on its immunosurveillance activity that suppresses tumor development and its progression. The complex interactions required for the immune system to influence tumor immunogenicity and tumor clonal selection process fuel the tumor mass to acquire immune-evasiveness that could overcome anti-tumor immune activity (Osisami & Keller, 2013). The whole process is comprised of three distinct stages: 1. elimination (the activation of innate and adaptive immunity that causes destruction of tumor cells), 2. equilibrium (tumor cells are subjected to balanced rates of proliferative activity and adaptive immune system's cytolysis), and 3. escape (uncontrollable proliferative activity of resistant tumor cells that are not susceptible to immunosurveillance; Dunn et al., 2004). Divergence of certain tumor clones that persisted and survived immune-destruction within a tumor mass, creates a subpopulation predominantly

comprised of cells with low immunogenicity and tumor-specific antigen expression (such as PD-L1). This surviving subpopulation enters an equilibrium phase, potentially remaining in a state of immune dormancy for decades (Osisami & Keller, 2013; Risson et al., 2020). On a cellular level, the rate of proliferative activity of these tumor cells is simultaneously counterbalanced by an equal rate of cell death instigated by the host's immunosurveillance system (Gomis & Gawrzak, 2017). The immune equilibrium hypothesis indicates that immunosurveillance mechanism controls the proliferative activity of DTCs through either T cell-mediated and/or NK cell-mediated cytolysis, or anti-idiotypic antibody networks that prevent tumor outgrowth. Concomitantly, immune cells can induce and promote immune dormancy using non-cytotoxic induction approach, via cytostatic molecules (such as IL12, INFγ, and TNF-mediated signaling; Eyles et al., 2010; Osisami & Keller, 2013; Risson et al., 2020; Wang & Lin, 2013). Escape from immunologic dormancy entails tumor cells to acquire mutations that can decrease its immunogenicity, attract immune-suppressive cells, and allow them to secrete factors (such as IL23) to dampen both the innate and adaptive immune responses (Wang & Lin, 2013).

1.2. Cellular (solitary) tumor dormancy

Cellular (solitary) tumor dormancy has been described as a reversible non-proliferative state where tumor cells are being arrested in the G_0 phase (Damen et al., 2021; Gomis & Gawrzak, 2017). Generally, this non-proliferative characteristic can be categorized by three partially overlapping cell cycle arrest mechanisms: quiescence, terminal differentiation, and senescence (Damen et al., 2021; Risson et al., 2020). Dormant tumor cells seem to share most commonalities with quiescent cells since their main common characteristic is the reversibility of the cell cycle arrest, meaning cells can re-enter the cell cycle and continue to proliferate after an extended period of inactivity (Coller et al., 2006). Dormant tumor cells, in comparison to quiescent cells, have additional epigenetic changes that allow them to maintain the cell cycle arrest for a longer time (Coller et al., 2006; Damen et al., 2021). Ultimately, both mechanisms have been shown to be causative for the survival of tumor cells during targeted therapy and chemotherapy – while maintaining the transcriptional plasticity required to reactivate and form new tumors upon favorable conditions (X. L. Gao et al., 2017; Osisami & Keller, 2013).

1.2.1. Intracellular cues

The main intracellular signaling pathways that define proliferation/dormancy status of tumor cells include the ratio between ERK1/2 and MAPK p38 (Aguirre-Ghiso et al., 2003). The ERK1/2 signaling cascade induces proliferation through the upregulation of cyclin D1 – a protein required to progress through the G_1 phase of the cell cycle (Lavoie et al., 1996). In contrast, the p38 pathway acts as an inducer of tumor cells to enter the G_0 phase by regulating stress signaling pathways and tumor suppressor pathways. This is mostly achieved through the upregulation of the cell cycle arrest proteins,

p16, p53, p21, and p27, as well as the activation of dormancy regulating transcription factors, e.g. NRF2F1, which promotes global chromatin repression and induces pluripotency factors (Aguirre-Ghiso et al., 2003; Damen et al., 2021; S. Y. Park & Nam, 2020; Recasens & Munoz, 2019). The general consensus is that dormant tumor cells are defined by the downregulation of phosphorylated ERK1/2 and the increased expression of phosphorylated p38, making p-ERK^{low} /p-p38^{high} phenotype distinct biomarker in predicting and identifying dormant state (Aguirre-Ghiso et al., 2003; Recasens & Munoz, 2019). Additionally, genetic studies have pointed out that tilting the balance between p-ERK1/2 and p-p38 towards p-ERK1/2 caused tumor cell reawakening from a permissive state, thus allowing cancer to relapse (S. Y. Park & Nam, 2020). Many other signaling pathways and networks have been proposed to have crucial roles in tumor dormancy, however most of them ultimately led to the modulation of p-ERK/p-p38 ratio, once again demonstrating that the ERK/p38 signaling is predominantly the current molecular basis of tumor dormancy and reawakening (Damen et al., 2021; X. L. Gao et al., 2017; Gawrzak et al., 2018; S. Y. Park & Nam, 2020).

1.2.2. mVenus-p27K$^-$ detection system of dormant tumor cells

Since there has been an increased amount of reports regarding tumor dormancy and that it should be considered as a dynamic rather than a static process, detection and isolation methods that precisely separate individual living cells in the G_0 from the G_1 state has become a key first step in its analysis (Montagner & Sahai, 2020). Thus, Oki et al. (2014) have developed a quiescent cell detection system that mainly targets the cyclin-dependent kinase inhibitor p27, which is known to inhibit cyclin-CDK (CDK1, 2, 4, and 6) complex that enables cell cycle progression from the G_0-G_1 and the G_1-S phase. p27 inhibitory activity is regulated on a post-translational level, using ubiquitination and proteasome degradation pathway via at least two different ubiquitin ligases – KPC that promotes p27 proteolysis at the G_0-G_1 transition, and SCF^{Skp2} that promotes p27 proteolysis at the S/G_2/M phase. Higher concentrations of p27 are mostly found in quiescent cells that are in the G_0 state as well as in a minor subpopulation of cycling cells whose cell cycle is paused at one of the regulatory checkpoints. Significant differences in the concentration levels of p27 between cycling cells and quiescent cells have made p27 a suitable molecular marker of dormant cells. To visualize cells in the G_0 phase, cells are subjected to stable transduction by inserting constitutively expressed gene that encodes a fusion protein – containing a fluorescent protein mVenus and a p27K$^-$ mutant lacking CDK inhibitory activity. The main advantage of this system is that it can be elevated and coupled with FUCCI probes and/or constitutively expressed fluorescent protein of different emission color (such as mCherry, dTomato etc.), providing a more detailed distinction between cells that are fully in the G_0 phase from those in the G_0-G_1 transition and the G_1 phase (Montagner & Sahai, 2020; Oki et al., 2014; Phan & Croucher, 2020).

1.2.3. Extracellular cues

Different types of tumors disseminate to occupy distinct metastatic niches – each characterized to have a unique molecular composition – which can induce dormancy through a variety of molecular mechanisms. Localization of DTCs upon extravasation in the secondary site influences the occurrence of dormancy as they immediately engage with the niche's paracrine signals (Summers et al., 2020). Dormant DTCs are often found near mature blood vessels as they have high depositions of the endothelium-derived tumor suppressor – TSP1. Bone marrow (BM) vascular niches secrete von Willebrand factor (vWF) to induce dormancy and chemoresistance in DTCs by activating integrin signaling (integrin β1 and/or integrin $\alpha_v\beta_3$). As well, BM perivascular mesenchymal stem cells (MSCs), stromal cells, and osteoblasts can secrete CXCL12, BMPs, and Wnt5a, respectively, to keep DTCs in a quiescent state (Agarwal et al., 2019; Kobayashi et al., 2011; Risson et al., 2020; Webster et al., 2015). In the lung, stromal cells secrete BMP4 to mediate cellular dormancy in breast cancer, thus preventing further metastatic outgrowth (H. Gao et al., 2012). The composition of the basement membrane is also known to highly influence direct interactions and signaling networks of adjacent tumor cells. Increased deposition of tumor cell-derived collagen COL3A1 in basement membranes around solitary DTCs has not only induced the cell cycle arrest in an autocrine manner, but also has influenced nearby DTCs to create a local dormant niche. Specifically, COL3A1 has been demonstrated to remodel microenvironmental architecture by reducing collagen fiber alignment and basement membrane stiffness, creating a more flexible and disorganized ECM – a known dormancy signature (Di et al., 2021). Another basement membrane factor implicated in dormancy is COL17A1 – a cell adhesion molecule that strengthens hemidesmosome interactions through the inhibition of FAK-YAP signaling axis – known to promote escape from dormancy (Ohta et al., 2022). Dormancy has also been correlated to the increased levels of DNA methylation and repressed chromatin after treatment, emphasizing epigenetic involvement in dormancy progression. Additionally, previously mentioned angiogenic dormancy activator miR-126 has also been proven to promote cellular dormancy. Endothelial cells and/or tumor cells have been shown to secrete miR-126 in BM vascular space and stimulate formation of quiescent pool of leukemic stem cells (LSC) with extended survival rates (Risson et al., 2020; Zhang et al., 2018; Figure 2).

1.3. DTC reactivation/Metastatic colonization

The perivascular space can contain tumor-promoting or -suppressive factors, primarily depending on the activity of endothelial cells and pericytes (Ghajar et al., 2013; Gomis & Gawrzak, 2017). DTCs have been shown to proliferate near neovascular sprouting points, where a dormancy cue TSP1 is reduced (Ghajar et al., 2013; Gomis & Gawrzak, 2017; Páez et al., 2012). These hot spots also contain elevated levels of tumor-promoting signals such as ECM molecules and growth factors, including active TGFβ1 and periostin (POSTN) that stimulate reawakening from dormancy and

metastatic outgrowth. Therefore, tip endothelial cells are considered to be areas of tumor reactivation, whereas stalk endothelial cells are known to promote dormancy (Ghajar et al., 2013). Apart from the mentioned TGFβ1 and POSTN factors, tumor reawakening in the perivascular niche can be mediated by L1 cell adhesion molecule (L1CAM) through the activation of YAP signaling. DTCs utilize L1CAM-YAP signaling as an essential factor in mimicking pericytes to enhance both cell proliferation and migration to spread and colonize lung capillaries (Er et al., 2018; Risson et al., 2020).

Outside of perivascular cells, several significant microenvironmental factors can drive tumor reactivation. Inflammatory-related neutrophil extracellular DNA traps (NETs) have been shown to reactivate dormant tumor cells through the release of neutrophil elastase and matrix metalloproteinase 9 (MMP9) enzymes. These enzymes promote ERK, FAK, and MLCK signaling networks, resulting in the upregulation of transcription factor YAP in malignant cells (Albrengues et al., 2018; J. Park et al., 2016; Risson et al., 2020). Also, overexpression of Coco protein at lung metastatic sites can cause reawakening of breast cancer cells by inhibiting dormancy cue BMP4 (H. Gao et al., 2012). ECM remodeling also seems to be a key mechanism of tumor reawakening since age-related cancer relapse was observed. Aging appears to reduce frequency of dormant tumor cells in BM niches since they exhibit higher expression levels of inflammatory cytokines that promote proliferation, while pro-dormancy factors (such as BMP4, BMP7, and TGFβ2) have displayed reduced expression. Furthermore, age-related remodeling of collagen matrix by forming stiffer collagen, has also stimulated metastasis in melanoma (Risson et al., 2020; Singh et al., 2019; Figure 2).

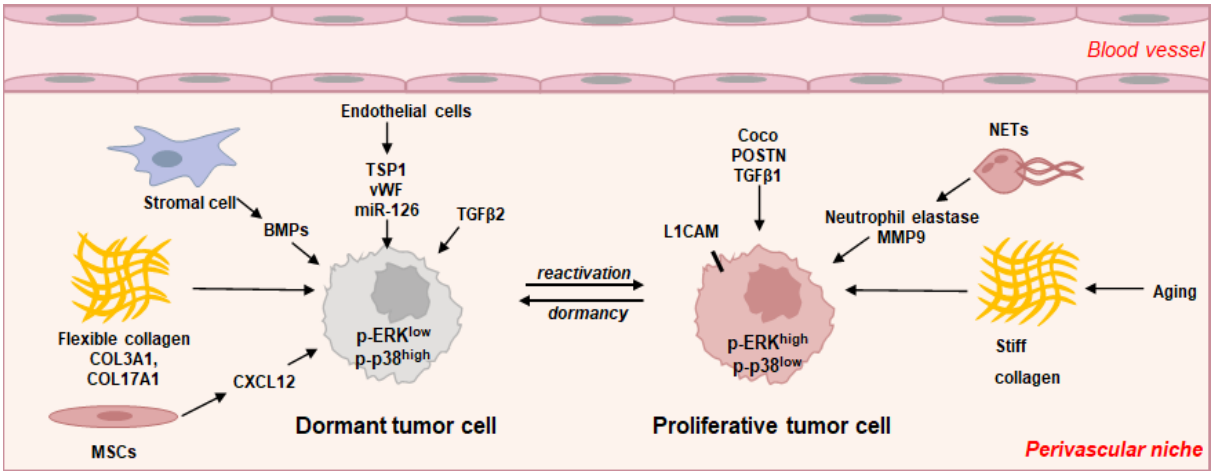

Figure 2. Extracellular and intracellular dormancy and reactivation cues in various perivascular niches (Figure created in Microsoft PowerPoint).

Dormancy is defined by p-ERK^{low}/p-p38^{high} and its influenced by dormancy cues, including TSP1, vWF, miR-126, TGFβ2, BMPs, CXCL4, COL3A1, COL17A1 etc. Reactivation/proliferation is defined by p-ERK^{high}/p-p38^{low} and its influenced by reactivation cues, including Coco, POSTN, TGFβ1, NETs, stiff collagen, and aging.

1.4. Dormancy and reactivation cues as adjuvants for cancer therapy

Dormancy and reactivation cues as potential adjuvants for personalized cancer therapy represent an initial step in targeting treatment-related relapse (S. Y. Park & Nam, 2020). In regards to that, there are two proposed pharmacological strategies that aim to inhibit residual tumors to relapse: 1. keeping dormant tumor cells in a quiescent state and 2. promoting tumor reactivation to create high-proliferative clones sensitized for chemotherapy (Ghajar, 2015). The former strategy is based on the notion that the identification of dormancy cues can help maintain DTCs in a dormant state to prevent metastatic relapse after surgical procedures, chemotherapy and/or radiotherapy. This "sleeping strategy" can sustain tumor dormancy by liberating tumor cells from the complete control of the external factors that can alter under conventional treatments. The main downsides of this approach are the inaccessibility to target all individual dormant tumor cells and the continuous toxic effects brought about by the life-long therapy strategy to always keep tumor cells clinically undetectable. The latter strategy is based on the rationale that identification of reactivation cues can support deliberate reawakening of dormant tumor cells to create high-proliferative tumor cells susceptible to conventional anti-proliferative treatments (such as chemotherapy and radiotherapy). However, concerns regarding this approach are mostly based on the fact that forceful stimulation of tumor outgrowth can cause uncontrollable and rapid proliferation which can ultimately result in advanced tumor development (Damen et al., 2021; Ghajar, 2015; S. Y. Park & Nam, 2020; Recasens & Munoz, 2019; Summers et al., 2020). Appropriate combination of dormancy and reactivation cues as well as establishing the most optimal timepoint for their application are crucial to increasing the potency of treatment-related relapse.

1.5. Multimerin 2/Endoglyx 1

Currently available treatments and therapeutic approaches that focus on targeting dormant tumor cells and recurring metastasis are quite unsuccessful, necessitating the identification of all potential molecular cues and mechanisms that govern tumor dormancy and reawakening (Damen et al., 2021).

In vitro and *in vivo* tumor dormancy experiments at the Max Planck Institute for Heart and Lung Research have assessed extracellular signaling cues present in the lung perivascular niche as they screened for dormancy-related genes. Conducted experiments have revealed that lung endothelium-related genes can be divided into two main group of genes associated with dormancy – reactivation hits and dormancy hits. Among major reactivation hits that have shown significant decrease in the number of metastatic lesions detected on lungs when eliminated was multimerin 2 (Unpublished; Figure 3a-f).

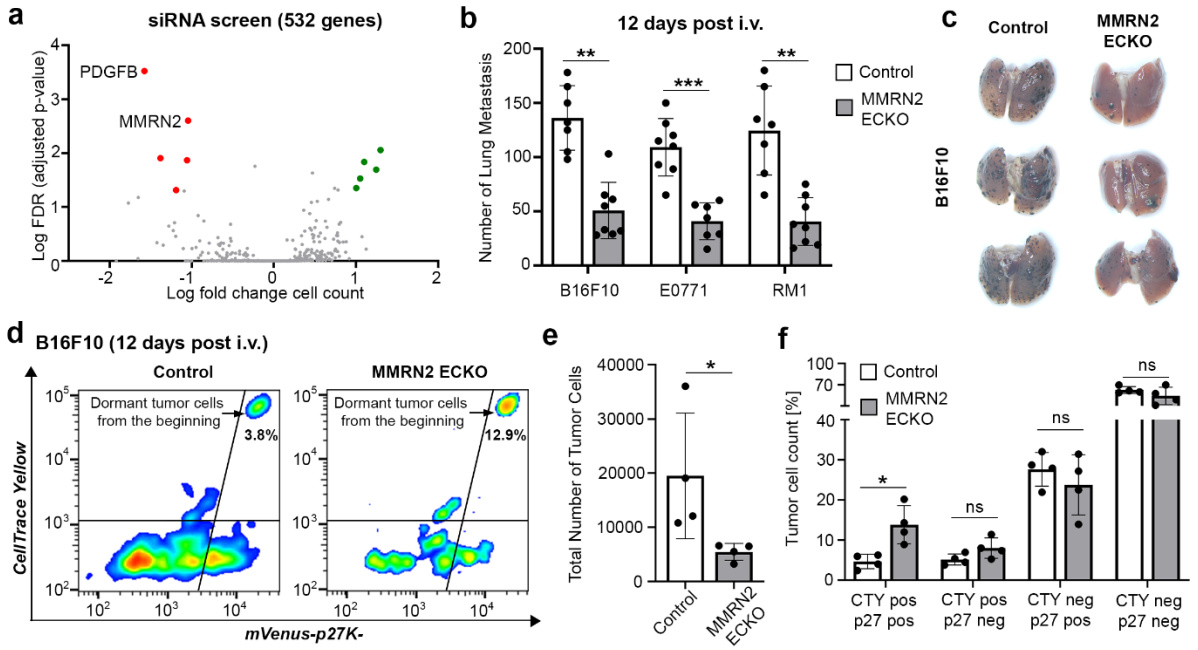

Figure 3. Multimerin 2 (MMRN2) promotes tumor reactivation and proliferation (Unpublished). (a) Graph depicts log fold changes in the tumor cell count after the siRNA screen for dormancy- and reactivation-related endothelial genes in the HUVEC-MDA-MB-231 co-culture system. (b) The bar diagram shows the number of lung metastasis 12 days post i.v. injection of B16F10, E0771, and RM1 in control and MMRN2 EC KO mice and (c) images of lung metastasis of B16F10. (d) Graph shows the number of subpopulations of B16F10 after sorting (using CellTrace Yellow (CTY) and mVenus-p27K$^-$) 12 days post i.v. injection in control and MMRN2 EC KO mice. (e,f) The bar diagrams show the total number of tumor cells and percentages of CTY-p27 subpopulations in control and MMRN2 EC KO mice.

Multimerin 2 (MMRN2)/endoglyx 1 is a 500 kDa extracellular matrix multimer glycoprotein, a representative member of the elastin microfibril interface-located (EMILIN) protein family which is comprised of various high molecular weight glycoprotein complexes (Christian et al., 2001a). MMRN2 has low expression levels and it is secreted by endothelial cells in both physiological and tumoral vasculature, particularly at points of neovascularization in certain types of tumors. MMRN2 is deposited along the blood vessels and it is localized in close proximity to endothelial cells (Christian et al., 2001a; Lorenzon et al., 2012).

1.5.1. MMRN2 structure and interaction partners

MMRN2 is comprised of three main domains: N-terminal EMI domain, central coiled-coil (CC) domain, and C-terminal complement component 1q (C1q) domain. The N-terminal EMI region – cysteine-rich domain is highly preserved among EMI-domain containing proteins and is involved in disulphide bridge formation. The CC region is comprised of the individual coiled-coil subdomains that are separated by the non-coiled regions, providing MMRN2 structural flexibility. This domain has an alpha-helical coil-coils forming a rod-like structure that has high tertiary structure homology among

protein family members. Located between the central region and the C1q domain is a small unique region in MMRN2 comprising an acidic arginine-rich region, however this structure varies among family members. At the C-terminal end, the C1q domain is located. In reducing conditions, protein's multimeric structure of 500 kDa is degraded to three heteromeric polypeptides with molecular weights of 125/140 kDa for major protein and around 110 kDa and 200 kDa for other proteins. Post-translational modifications, such as N- and O-glycosylations, were confirmed in all subunits of the protein complex (Christian, Ahorn, Novatchkoval, et al., 2001; Colombatti et al., 2012).

The multidomain structure of MMRN2 allows the simultaneous binding of interaction partners closely related to their tight juxtaposition with endothelial cells in the blood vasculature. It has been confirmed that the CTLD group 14 family members CLEC14A and CD93 directly bind MMRN2 through non-glycosylated segment of CC region. Additionally, TEM1 expressed in fibroblasts and/or pericytes has also proven to interact with MMRN2 through its CC region, but its binding domain was determined to be completely different than the one required to interact with CLEC14A and CD93. Eventually, it has been demonstrated that simultaneous interaction and co-localization of CLEC14A/CD93 and TEM1 with MMRN2 is present in the perivascular niche, specifically at the interface between endothelial cells and TEM1-positive cells (most likely fibroblasts or pericytes; Khan et al., 2017; Noy et al., 2015). As well, MMRN2 has been demonstrated to interfere with VEGFA/VEGFR2 interaction on the surface of the endothelial cells by binding to VEGFA that decreased VEGFR2 phosphorylation and downstream signaling factors (Lorenzon et al., 2012).

1.5.2. MMRN2 function in tumorigenesis

MMRN2 has been implicated in angiogenesis and tumor growth, however several studies have shown contradictory outcomes which makes its exact effect on tumor growth unclear. Depending on the analysis of individual interactions that MMRN2 exerts in conditions isolated from other ECM factors, it seems that it can exhibit both pro- and anti-tumorigenic functions (Khan et al., 2017). MMRN2 has been shown to impair angiogenesis through binding directly to the angiogenic factor VEGFA, which sequesters and inhibits it from binding and activating VEGFR2. MMRN2-positive cells failed to effectively grow well-vascularized tumors, thus preventing further steps in metastatic cascade (Colladel et al., 2016; Khan et al., 2017; Lorenzon et al., 2012). On the other hand, many studies have described MMRN2 as a pro-angiogenic molecule since MMRN2 is known to interact with transmembrane proteins (such as CLEC14A, CD93 and TEM1), thus stabilizing adhesion between endothelial cells and pericytes and promoting vessel formation and maturation. Also, the MMRN2-TEM1 interaction can stimulate proliferation of pericytes and fibroblasts and thus act in a pro-angiogenic manner, supporting tumor outgrowth and metastasis (Khan et al., 2017; Noy et al., 2015; Zanivan et al., 2013). Currently, the role of MMRN2 in tumorigenesis is hard to predict and is suggested to depend on its concentration, localization and interaction with other components in the intercellular space.

1.6. Tumor endothelial marker 1/Endosialin/CD248

As MMRN2 was screened to be a reactivator using *in vitro* and *in vivo* tumor dormancy models by the Metastasis group at the Max Planck Institute for Heart and Lung Research (Unpublished), they tried to check which of the known receptors of MMRN2 is present and/or upregulated in metastatic tumor clones that have homed in the lung.

Dormant and metastatic tumor clones were sorted clonally using single-cell sorting of both GFP to identify tumor cells and CellTrace Far Red (CTFR) to delineate dormant cells from proliferating cells. The $GFP^{pos}CTFR^{high}$ subpopulation was considered to contain dormant tumor cells while the $GFP^{pos}CTFR^{neg}$ subpopulation were the metastatic clones (Figure 4a). These clones were validated by reinjecting them in mice via the intravenous route and it was observed that the dormant clones barely developed any lung metastasis while the metastatic clones had more lung metastasis than the parental ones. Upon intranasal administration of lipopolysaccharide (LPS), these dormant metastasis reactivated *in vivo* – establishing that the cell cycle arrest observed is reversible and can be attributed to dormancy/quiescence (Figure 4b,c). RNA-sequencing analysis of these dormant and metastatic clones revealed that TEM1, but not CLEC14A and CD93, was sufficiently present (>100 RNA-seq reads) and upregulated in the metastatic clones (Figure 4d). Since MMRN2 is present in the perivascular niche irrespective of the presence of tumors, it is hypothesized that presence of TEM1 offers a selective advantage for tumor cells to colonize the lung (Unpublished).

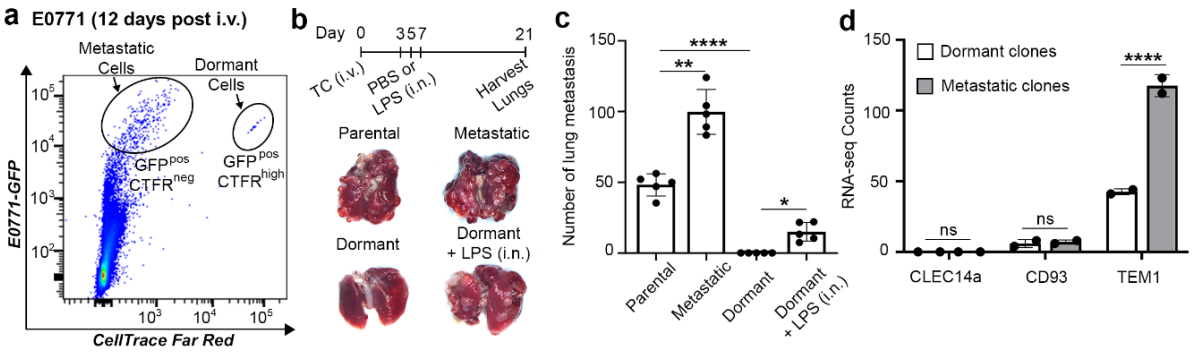

Figure 4. TEM1 is upregulated in the metastatic clones of E0771 (Unpublished).

(a) Graph depicts a density plot of subpopulations of E0771 after sorting lungs (using GFP and CellTrace Far Red (CTFR)) 12 days post i.v. injection in mice. (b) Image represents lung metastasis after reinjecting parental, metastatic, and dormant tumor clones with i.n. additions of PBS or LPS 21 days post i.v. injection in mice and the bar diagram (c) show quantified number of lung metastasis. (d) The bar diagram shows quantified RNA sequencing results of CLEC14a, CD93, and TEM1 in the dormant and metastatic tumor clones.

Tumor endothelial marker 1 (TEM1)/endosialin/CD248 is a representative member of the C-type lectin domain (CTLD) group 14 family which is comprised of highly glycosylated transmembrane receptor proteins including the well described CLEC14A, CD93, and thrombomodulin proteins (Khan

et al., 2019; Kondo et al., 2022). TEM1 was initially classified as a tumor vasculature endothelium biomarker, however it was later demonstrated that TEM1 is actually not expressed by the endothelium, but rather is present on pericytes and tumor associated fibroblasts as well as some tumor cells of multiple tumor types (Teicher, 2019; Valdez et al., 2012).

1.6.1. TEM1 structure and interaction partners

TEM1/endosialin/CD248 is a highly glycosylated, type I transmembrane receptor protein which consists of six functional domains, whose core molecular weight in humans is 95 kDa. Since the protein is subjected to many post-translational modifications (mostly O-glycosylations and to a smaller extent phosphorylations and potential N-glycosylations), it is expected that its molecular weight will increase to approximately 165 kDa depending on the degree of modifications (Christian et al., 2001a; Rettig et al., 1992). Structurally, TEM1 is considered to be a prototypical member of the CTLD group family 14, exhibiting standard general structure representative for most transmembrane multidomain proteins (Khan et al., 2019). An extracellular N-terminal region of TEM1 is comprised of five globular domains. First region is the CTLD – an ectodomain that is architecturally homologous among the members of this protein family. Second region is the Sushi-like domain which is an extracellular motif involved in diverse protein-protein interactions. Adjacent region includes three consecutive EGF-like domains which are conserved tandem repeats that can be found in a broad spectrum of proteins. Furthermore, the extracellular juxtamembranous region (also referred to as the mucin-like region) is enriched with polar amino acids, specifically serine, threonine, and proline residues, providing docking points for many O-linked sialylated oligosaccharides. Structural models have revealed that human TEM1 contains 27 O-glycosylation sites that are directly involved in proper folding, ligand interactions, and preventing protein from the potential access of extracellular proteases to the protein core. Additionally, TEM1 is integrated into the plasma membrane via the single pass hydrophobic transmembrane domain that is connected to the highly conserved long cytoplasmic tail. Its intracellular C-terminal domain is comprised of three phosphorylation sites and C-terminal PDZ-motif that in many homologous transmembrane proteins act as an adaptor molecule and provide scaffolding function with specific docking points for many intracellular proteins (Christian et al., 2001a; di Benedetto et al., 2019; Maia et al., 2011; Opavsky et al., 2001; Valdez et al., 2012).

Multidomain architecture of the extracellular region of TEM1 has indicated that TEM1 has several interaction partners that influence its cellular function. The CTLD ectodomain of TEM1 selectively binds fibronectin and collagens type I and IV which highly influence promotion of cell attachment, adhesion and migration during tumor invasion. Consequently, TEM1 upregulates MMP9 that leads to ECM degradation – a crucial factor in tumor invasion, angiogenesis, and metastasis (Brian et al., 2007; di Benedetto et al., 2019). TEM1 can also bind to Mac-2BP leading to higher metastatic dissemination of tumor cells and decreased survival rates (Cesinaro et al., 2002; Khan et al., 2019).

Furthermore, the CTLD region of TEM1 interacts with endothelial ECM protein MMRN2, which is secreted along blood vessels and thus have either pro- or anti-angiogenic function depending on the state of tumor vascular formation. Fibroblasts and/or pericytes expressing TEM1 can co-localize with endothelial cells expressing CD93 via MMRN2 as an "extracellular glue" between two receptors (Khan et al., 2017). Intracellular domain of TEM1 has been shown to be involved in the promotion of tumor development and growth in mouse models, however interaction partners have not yet been discovered. As previously mentioned, computational prediction models have revealed that cytoplasmic tail contains three potential phosphorylation sites and the PDZ domain that represent possible points of interaction with intracellular factors, opening the possibility for potential signal transduction between extracellular ligands and downstream molecules, however the existence of these factors remains elusive (Khan et al., 2019; Opavsky et al., 2001; Valdez et al., 2012).

1.6.2. TEM1 function in tumorigenesis

The role of TEM1 in tumorigenesis is directly associated with its increased expression in perivascular cells (such as pericytes, fibroblasts) and malignant cells of various tumor types navigating the metastatic cascade through cellular proliferation, invasion, and migration (di Benedetto et al., 2019; Kondo et al., 2022; Maia et al., 2011; Valdez et al., 2012). Absence of TEM1 has proven to cause a reduction in the rate and the size of tumor growth, but also an increase in tumor vascularization. This discrepancy between tumor growth and tumor-induced vascular patterning still remains unexplained, however few assumptions have been proposed including that TEM1 seems to mediate a key role in the vasculature regression. While its removal potentially promotes sprouting of small blood vessels, its presence is still necessary for vessel maturation. As well, TEM1 deficiency may cause alterations in the release of stroma-derived factors (such as ECM proteins, MMPs, and growth factors) that participate in angiogenesis (di Benedetto et al., 2019; Khan et al., 2019; Maia et al., 2011). Additionally, the upregulation of TEM1 in stromal cells have individually increased metastasis by promoting tumor cell invasion and intravasation via previously mentioned interactions (Liu et al., 2021). Even though intracellular interaction partners of TEM1 are still unknown, TEM1 has been indirectly found to positively mediate the PDGFR signaling pathway, inducing proliferative and migratory ability of pericytes and fibroblasts (Tomkowicz et al., 2010). At the same time, TEM1 has been hypothesized to negatively mediate Notch3 signaling, thus resulting in a decrease of proteins with tumor suppressor properties and an increase of MMPs. Additionally, TEM1 has been shown to influence promotion of HIF1 transcription, consequently increasing levels of VEGF and VEGFR1 among other key factors. These observations in mural cells and fibroblasts led to tumor growth and inflammation (Maia et al., 2011; Valdez et al., 2012).

2. AIMS OF THE STUDY

The main objectives of this master's thesis research project include:

1. functional analyses of TEM1 and its implications in basal tumor characteristics *in vitro*
2. assessing how tumor cells expressing TEM1 and endothelial cells expressing MMRN2 jointly influence both tumor dormancy and reactivation processes during their co-localization *in vitro*
3. functional analyses of TEM1 in lung metastasis *in vivo*

The main hypothesis of this research is that the upregulated TEM1 expression in B16F10 melanoma and E0771 breast cancer cells is an essential factor in lung metastasis and that the co-localization of endothelial cells and tumor cells is necessary for the MMRN2-TEM1 interaction to occur and activate the ERK1/2 pathway. Positive regulation of the MMRN2-TEM1 signaling pathway potentially represents a molecular basis in promoting tumor cell proliferation, causing DTC reawakening and recurrence of residual tumor disease in cancer patients. It is thus hypothesized that TEM could act as a prediction marker for poor prognosis in cancer patients.

3. MATERIAL AND METHODS

3.1. Material

3.1.1. Cells

Human umbilical vein endothelial cells (HUVECs) and Mouse lung endothelial cells (MLECs) were purchased from Lonza and Pelobiotech, respectively. HUVECs were cultured using EGM-2 (Lonza) and MLECs were cultured using EGM-2-MV (Cell Biologics). B16F10 melanoma and E0771 breast cancer cells were purchased from ATCC and Cell Biologics. HEK293T was purchased from ATCC. All tumor cell lines and HEK293T were cultured using DMEM supplemented with 10% FBS, L-glutamine (1x; Thermo Fisher Scientific). Cells were tested negative for mycoplasma contamination before experiments.

Cells that were stored at -80 °C were thawed at 37 °C in warm bath. Samples were transferred to 5 mL of appropriate media and centrifuged at 300 x g for 3 min at room temperature. Supernatant was removed and pellet was resuspended in corresponding media before transferring in 10 cm Petri dishes. Endothelial cells were transferred into plates that had previously been coated in 1% collagen type I (Corning) in 0.1% acetic acid (Carl Roth) for 30 min at room temperature and washed with PBS (1x; Thermo Fisher Scientific). Cells were cultured at 37 °C with 5% CO_2 in an incubator.

Determining cell concentration before conducting an experiment was done by removing appropriate media from 10 cm Petri dishes and washing cells with PBS (1x; Thermo Fisher Scientific). Cells were trypsinized using 0.25% Trypsin-EDTA (Thermo Fisher Scientific) for at least 2 min – until cells have completely detached – at 37 °C with 5% CO_2 and recovered with media. Cells were centrifuged at 300 x g for 3 min at room temperature and supernatant was removed. Appropriate media was added to pellet and samples were resuspended. Aliquot was added to Bürker-Türk hemocytometer counting chamber and cells were manually counted.

Storage of remaining cells was conducted by mixing cells with 95% FBS (Thermo Fisher Scientific) supplemented with 5% DMSO. Cells were centrifuged at 300 x g for 3 min at room temperature and supernatant was removed. Freezing media (95% FBS + 5% DMSO) was added to cells and samples were transferred to 5 mL vials. Samples were stored at -80 °C.

3.1.2. Experimental mice

Wildtype C57BL6/J mice (Jackson Laboratory) were used for the primary tumor growth, resections, extravasation, and lung metastasis assays. All procedures involving animal care and use in this study were approved by the local animal ethics committee of the Regierungspräsidium Darmstadt under the B2-1175 proposal, and were done by supervisor. Mice were housed under a 12-hour light/12-

hour dark cycle, with free access to food and water and under specific pathogen-free conditions unless stated otherwise.

3.2. Methods

3.2.1. mCherry:mVenus-p27K$^-$ detection system

mCherry:mVenus-p27K$^-$ detection system of dormant tumor cells is based on a stably transduced tumor cell line with *mCherry* and *mVenus-p27K$^-$* genes. mCherry was used to visualize and differentiate all tumor cells, regardless of their proliferative status, from surrounding cells, since mCherry is constitutively expressed and localized in cytoplasm of tumor cells, emitting a red fluorescent color. On the other hand, the localization of mVenus-p27K$^-$ fusion protein in nuclei of just non-proliferative tumor cells provide additional green fluorescence to the already existing cytoplasmic red fluorescence from mCherry, exclusively marking a dormant subpopulation of tumor cells (Figure 5).

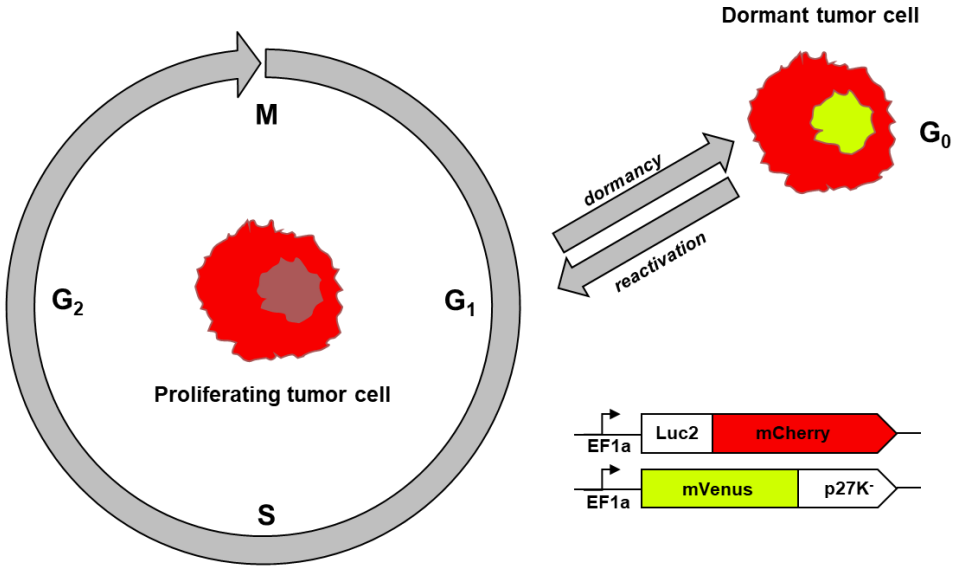

Figure 5. mVenus-p27K$^-$ detection system of tumor dormancy (Figure created in Microsoft PowerPoint). Tumor cell lines containing mVenus-p27K$^-$ detection system are based on a stable transduction of *mCherry-Luciferase (Luc2)* and *mVenus-p27K$^-$* genes, both regulated by EF1a promoter that has constitutive activity. System is based on a differential expression of p27 mutant cyclin-CDK inhibitor that is predominantly present in the G_0 phase of the cell cycle. Proliferating tumor cells thus express red fluorescent color emitted from mCherry in the cytoplasm, while dormant tumor cells express both red and green fluorescent color emitted from mCherry in the cytoplasm and mVenus-p27K$^-$ from the nucleus, respectively.

3.2.2. Lentiviral transduction

To generate tumor cell lines with stable TEM1 knockdown and/or in which mCherry-Luciferase: mVenus-p27K$^-$ system was integrated, the lentiviral vectors containing *shScr*, *shTEM1*, *mVenus-p27K*$^-$, and *mCherry-Luciferase* were used. Vector structures and inserted sequences used in the experiment are described in detail in Supplementary material.

B16F10 and E0771 tumor cell lines were cultured until 70% confluent. Cells were transfected with psPax2 and pCAG-Eco (Addgene) alongside the appropriate knockdown or overexpression vectors by using Opti-MEM (Thermo Fisher Scientific) and Lipofectamine 3000 (Invitrogen) protocol according to the manufacturer's instructions. After 24 h of incubation at 37 °C at 5% CO_2, media was carefully changed. After another 24 h, supernatant was collected and subjected to a centrifugation at 300 x g for 3 min at room temperature. Supernatant was filtered through a low protein binding filter (0.45 μm; Sartorius) and 1/3 of the volume of Lenti-X-concentrator (Takara) was added, followed by gentle agitation until mixture became homogenous. Mixture was incubated for 24 h at 4 °C. Mixture was centrifuged at 1500 x g for 45 min at 4 °C. Supernatant was removed and pellet was resuspended in 1.5 mL of warm media (DMEM + 10% FBS, L-glutamine (1x); Thermo Fisher Scientific) with 3 μg/mL polybrene (Merck), followed by vortex and incubation for 30 min at room temperature. 400 μL of virus mixture was combined with 200 μL of tumor cells (1.8 x 10^5 cells/well), and prepared samples were seeded onto 12 well plates and cultured at 37 °C with 5% CO_2. After 24 h, media was carefully changed. After 96 h, transduced tumor cells were trypsinized using 0.25% Trypsin-EDTA (Thermo Fisher Scientific) for 2 min at 37 °C with 5% CO_2 and recovered with media. Cells were transferred into 10 cm Petri dishes and 10 mL of media was added supplemented with puromycin (10 μg/mL; Sigma). Media was changed every 2 days and selection was terminated when all non-transduced cells were dead. Efficiency of viral transduction was assessed using quantitative real-time polymerase chain reaction (q-RT-PCR) and Western blot.

3.2.3. Quantitative real-time polymerase chain reaction (q-RT-PCR)

Total RNA extraction from tumor cells was conducted using Quick-RNA Micro Prep kit (Zymo Research) according to the manufacturer's instructions. Complementary DNA (cDNA) synthesis was performed using the ProtoScript II Reverse Transcription kit (New England BioLabs). Quantitative real-time PCR was carried out using 5 μL of cDNA samples (diluted in 200 μL deionized H_2O) and 15 μL of the Mastermix (TEM1 and GAPDH) prepared accordingly – 0.1 μL forward primer (Sigma), 0.1 μL reverse primer (Sigma), 0.2 μL hydrolysis probe (Roche Diagnostics), 10 μL Probes Master (Roche Diagnostics), and 4.6 μL deionized H_2O. The sequences for the primers are as follows:

GAPDH forward primer: 5'-AGCTTGTCATCAACGGGAAG-3'

GAPDH reverse primer: 5'-TTTGATGTTAGTGGGGTCTCG-3'

TEM1 forward primer: 5’-TTCCAGAGCCCCTCTAGTCC-3’

TEM1 reverse primer: 5’-AGCTGTGGCACTGATTTGG-3’

Samples were analyzed using Light-Cycler 480 Probe Master System (Roche). Each sample was analyzed in duplicates and GAPDH was used as an endogenous control. Relative expression was calculated using the ΔΔCt method.

3.2.4. Glycoprotein deglycosylation

Isolated protein samples were subjected to deglycosylation using O-Glycosidase and Neuraminidase Bundle kit (New England Biolabs) according to the manufacturer’s instructions. Samples were incubated for 6 h at 37°C in warm bath. Deglycosylated samples were stored at -20 °C.

3.2.5. Western blot

Total protein extraction from tumor cells was conducted using 65 µL RIPA Lysis and Extraction Buffer (Thermo Fisher Scientific) supplemented with 0.65 µL Protease/Phosphatase Inhibitor Cocktail (100x; New England BioLabs). The cells were treated with prepared ice-cold lysis buffer and incubated for 30 min on ice. The cell lysates were stored at -20 °C.

Laemmli Sample Buffer (4x; Bio-Rad Laboratories) was added to cell lysates and boiled for 10 min at 99 °C. Sample lysates were then subjected to SDS-PAGE. As a marker of molecular weights, PageRuler Plus Prestained Protein Ladder (Thermo Fisher Scientific) was used. SDS-PAGE was performed using Running Buffer (1x; Thermo Fisher Scientific) for 90 min at 120 V.

Protein blotting onto nitrocellulose membrane (Fisher Scientific) was conducted using Transfer Buffer (1x; Thermo Fisher Scientific) for 120 min at 300 mA. Membranes (Fisher Scientific) were washed three times for 10 min in TBST (20 mM Tris (Sigma), 150mM NaCl (Carl-Roth), 0.1% Tween 20 (Merck)) and blocked using 5% BSA (Biomol) for 30 min at room temperature while shaking. After blocking, membranes were subjected to incubation with gentle agitation at 4 °C overnight using following primary antibodies (dilution 1:2000): anti-TEM1 (Thermo Fisher Scientific, BS-2101R), anti-p-ERK1/2 (Cell Signaling), anti-ERK (Cell Signaling), anti-p27 (Thermo Fisher Scientific, PA5-27188), anti-α-tubulin (Cell Signaling), and anti-GAPDH (Cell Signaling). Membranes were washed three times with TBST (20 mM Tris (Sigma), 150mM NaCl (Carl-Roth), 0.1% Tween 20 (Merck)) and then incubated with HRP-conjugated secondary (New England Biolabs) antibody (dilution 1:1000) for 60 min at room temperature on a rotator. After second incubation, membranes were washed using TBST (20 mM Tris (Sigma), 150mM NaCl (Carl-Roth), 0.1% Tween 20 (Merck)). Finally, proteins of interest labeled with antibodies were chemiluminescently detected with ChemiDoc MP illuminator (Bio-Rad) using ECL Western Blotting Substrate (Thermo Fisher Scientific) according to manufacturer’s instructions. Band intensities obtained by immunoblotting were analyzed and quantified using ImageJ.

3.2.6. Proliferation assay

2 x 10^2 tumor cells/well were seeded onto 96-well plates. Tumor cells were incubated for 96 h at 37 °C with 5% CO_2 after which they were subjected to two different proliferation detection methods – EdU and Ki67.

EdU experiment was conducted using Click-iT Edu Imaging Kit (Invitrogen) with modifications from the manufacturer's instructions. 60 µL of prepared EdU (dilution 1:10 000) was added to each well and incubated for 6 h at room temperature. Cells were washed in PBS (1x; Thermo Fisher Scientific) and were fixed using 4% paraformaldehyde (PFA; Merck) for 10 min at room temperature on a shaker and permeabilized using 0,1% TRITON X-100 (Sigma-Aldrich) for 10 min at room temperature on a shaker. Cells were subsequently subjected to 5% BSA blocking solution (Biomol) for 10 min at room temperature on a shaker. After cells were washed two times with PBS (1x; Thermo Fisher Scientific) followed by 10 min incubation at room temperature with agitation, cells were subjected to Click-iT reaction cocktail (Invitrogen) prepared according to the manufacturer's instructions. 60 µL was added to each well for 30 min at room temperature on a shaker, protected from light. After washing two times with PBS (1x; Thermo Fisher Scientific), Hoechst (dilution 1:10 000; Thermo Fisher Scientific) was used to label cell nuclei for 15 min at room temperature, protected from light. Tumor cells were washed in PBS (1x; Thermo Fisher Scientific) and subjected to fluorescent microscopy using Olympus X. Images obtained by fluorescent microscopy were analyzed and quantified using ImageJ.

Ki67 experiment was conducted using immunocytochemistry method. Fixation, permeabilization and blocking reactions were performed using the same protocol as in EdU experiment (Invitrogen) according to the manufacturer's instructions. Immunostaining of Ki67 marker was conducted utilizing anti-Ki67 primary antibody (dilution 1:200; Invitrogen) and incubated overnight at 4 °C. After the same washing process, bound primary antibody was detected using Alexa Fluor 544-conjugated secondary antibody (dilution 1:500; Invitrogen) for 1 h at room temperature on a shaker. Further staining and visualization protocols were performed as in EdU experiments.

3.2.7. Apoptosis assay

5 x 10^4 cells/well were seeded onto 24-well plate. Tumor cells were cultured for 24 h at 37 °C with 5% CO_2 after which they were subjected to two different experiments – uninduced and induced apoptosis experiment.

In induced experiment, cells were treated with 5 µL of apoptotic inducer – staurosporine (10 $\mu moldm^{-3}$; Sigma-Aldrich) for 6 h in 37 °C with 5% CO_2, while in uninduced set, cells were treated with 5 µL of PBS (1x; Thermo Fisher Scientific). After incubation, suspension containing detached cells was transferred to tubes and wells were washed with PBS (1x; Thermo Fisher Scientific) and washing solution was transferred to the exact same tubes. Moreover, attached cells were trypsinized using 0.25%

Trypsin-EDTA (Thermo Fisher Scientific) for 2 min at 37 °C with 5% CO_2 and recovered with media (DMEM + 10% FBS, L-glutamine (1x); Thermo Fisher Scientific), transferring all remaining samples to the existing tubes. Tubes were eventually comprised of the attached and detached cells and subjected to centrifugation for 3 min at 300 x g at room temperature. Supernatant was removed and cells were stained using SYTOX AADvanced Dead Cell Stain Kit (Invitrogen) according to the manufacturer's instructions. 250 µL of reaction mix was added to each tube, vortexed and incubated for 20 min at room temperature. 250 µL of media and 1 µL of DAPI (Thermo Fisher Scientific) were added to each tube. Samples were resuspended and filtered before they were subjected to flow cytometry using BD FACSMelody Cell Sorter (BD Biosciences).

3.2.8. Migration assay

3 x 10^5 cells/well were seeded onto a 24-well plate. Tumor cells were cultured at 37 °C with 5% CO_2 until monolayer was formed. After reaching confluence, media (DMEM + 10% FBS, L-glutamine (1x); Thermo Fisher Scientific) was removed and vertical scratch was created across each well using ruler and pipette tip. PBS (1x; Thermo Fisher Scientific) was added to the sides of each well to remove scratched cells while not disturbing remaining tumor cells. After washing, media was added to the sides of remaining cells and cells were subjected to 16 h time-lapse incubation at 37 °C with 5% CO_2 using live-cell imaging microscopy (Olympus). Two images depicting upper and lower segments of each well were taken every 1 h for total of 16 h.

3.2.9. Transwell migration assay

The transwell (Corning) was coated with 1% collagen type I (Corning) in 0.1% acetic acid (Carl Roth) for 30 mins at room temperature. The transwell was washed with PBS (1x; Thermo Fisher Scientific) prior to seeding of HUVECs with a density of 1 x 10^5 cells/mL. After 48 h, tumor cells were seeded on top to the transwell and media (DMEM + 10% FBS, L-glutamine (1x); Thermo Fisher Scientific) was added on the outer part of the transwell. The plate was then incubated for 24 h at 37 °C with 5% CO_2. The transwell was then washed with PBS (1x; Thermo Fisher Scientific) and the inner part was cleaned with a cotton swab. The number of transmigrated GFP-labelled tumor cells were quantified using imaging with Olympus X.

3.2.10. siRNA-mediated knockdown

Endothelial cells were seeded onto 6-well plate and cultured until 70% confluent. Cells were transfected with siRNAs by using Opti-MEM (Thermo Fisher Scientific) and Lipofectamine RNAiMAX (Invitrogen) protocol according to the manufacturer's instructions. Scrambled siRNA control (siScr; sequence undisclosed; Qiagen) while mouse-specific MMRN2 siRNA (Sigma) used was SAS1_Mmo1_00130930 HA12284742.

3.2.11. Recombinant protein expression and concentration

To generate recombinant MMRN2 fragments (since whole MMRN2 is too large to be secreted *in vitro*): MMRN2$^{(128-487)}$-Fc and MMRN2$^{(487-814)}$-Fc, plasmid vectors containing Fc, MMRN2$^{(128-487)}$-Fc, and MMRN2$^{(487-814)}$-Fc were used. Vector structures and inserted sequences used in the experiment are described in detail in Supplementary material.

1.5 x 10^7 HEK293T cells were plated onto 10 cm Petri dishes that were coated with Poly-Lysine (33 µg/mL; Sigma) for 30 min. After 24 h, cells were transfected with 30 µg of plasmid using calcium phosphate method (Thermo Fisher Scientific) according to the manufacturer's instructions. 24 h post transfection, samples were gently washed two times with 30 mL serum-free media (DMEM + L-glutamine (1x); Thermo Fisher Scientific) and then replaced with 30 mL Opti-MEM (Thermo Fisher Scientific). After 48 h, supernatant containing secreted recombinant protein of interest was gently collected and combined with proteins from cells containing the same plasmid. Samples were centrifuged at 400 x g for 5 min at 4°C after which the supernatant was transferred to pre-chilled tubes and protease inhibitor cocktail (Thermo Scientific) were added. 500 µL of supernatant aliquot was stored at -20 °C for electrophoresis analysis.

15 mL of supernatant was transferred to Ultra-15 Centrifugal Filter Units 10 kDa cutoff (Amicon). Filter membrane was previously soaked in deionized H_2O and centrifuged at 4000 x g for 2 min at 4 °C after which water was removed from filter and collection tube. Filters were put on ice and kept wet. 10 kDa filter units were centrifuged at 4000 x g for 10 min at 4 °C and flow through was discarded. The rest of the supernatant was added to centrifugal filter unit and 10 kDa filter units were centrifuged at 4000 x g for another 20 min at 4 °C. Concentrate was collected from the filter. Centrifugal filter unit was washed and filled with deionized H_2O and stored at 4 °C since the column would be reused for the same protein purification later. 100 µL concentrate aliquot was stored at -20 °C for electrophoresis analysis. pH was also measured to be around 7, confirming that concentrate solution has adequate pH and that buffer exchange is not necessary.

3.2.12. Recombinant protein purification and quantification

Before purification of Fc, MMRN2$^{(128-487)}$-Fc, and MMRN2$^{(487-814)}$-Fc recombinant protein fragments, two collection tubes were prepared per one column and 30 µL of neutralizing buffer (Qiagen) was added to each. Collection tubes were kept on ice. Protein A HP spin trap columns (Qiagen) were taken and media inside the column was resuspended by inverting the columns. Storage solution was removed from the columns by centrifugation at 100 x g for 30 s at 4°C. To equilibrate columns, 600 µL of binding buffer was added. Columns were centrifuged at 100 x g for 30 s at 4 °C and flow through was discarded. To bind recombinant Fc protein to Protein A sepharose columns, 600 µL of supernatant concentrate was added after which top and bottom column caps were closed. Columns were incubated

for 15 min at room temperature with gentle agitation. Caps were opened and sepharose columns were centrifuged at 100 x g for 30 s at 4 °C and flow through was discarded. Same procedure was repeated until all concentrates were used. Sepharose columns were then washed four times using 600 µL of binding buffer, followed by centrifugation at 100 x g for 30 s at 4 °C after which flow through was discarded. Elution was conducted by adding 400 µL of elution buffer and inverting the sepharose columns several times. Columns were then placed in 2 mL collection tubes containing 30 µL neutralizing buffer, centrifuged at 70 x g for 30 s at room temperature and eluate was collected. Procedure was repeated using new collection tube. 100 µL of eluate aliquot was stored at -20 °C for electrophoresis analysis. Eluate buffer was exchanged with cold PBS (1x; $CaCl_2$ free, $MgCl_2$ free; Thermo Fisher Scientific) using small 10 kDa columns (Amicon) by refilling them six times with PBS (1x; Thermo Fisher Scientific) and centrifuging at 14 000 x g for 10 min at 4 °C each time. Obtained concentrate was collected and resuspended in 100 µL of PBS (1x; Thermo Fisher Scientific) for each 10 mL of starting cell supernatant.

Several concentrations of BSA (Biomol) in PBS (1x; Thermo Fisher Scientific) were prepared accordingly: 500 µg/mL, 250 µg/mL, 125 µg/mL, 62.5 µg/mL, and 31.25 µg/mL. Laemmli Sample Buffer (4x; Bio-Rad Laboratories) was added to 30 µL of BSA concentrations and boiled for 10 min at 99 °C. 20 µL of BSA samples were loaded per well containing: 7.5 µg, 3.750 µg, 1.875 µg, 0.9375 µg, and 0.46875 µg BSA, respectively.

Laemmli Sample Buffer (4x; Bio-Rad Laboratories) was added to samples and boiled for 10 min at 99 °C. Sample lysates were then subjected to SDS-PAGE. As a marker of molecular weights, PageRuler Plus Prestained Protein Ladder (Thermo Fisher Scientific) was used. SDS-PAGE using 10% acrylamide gels was performed using Running Buffer (1x; Thermo Fisher Scientific) for 90 min at 120 V. Gel was stained with Commassie (Bio-Rad) for 1 h at room temperature on a shaker. After incubation, gel was washed three times using acetic acid (Carl Roth). Incubation times were 30 min for the first two times and 1 h for the last time at room temperature on a shaker. Obtained bands for determining BSA (Bio-Rad) standard curve and proteins of interest were analyzed and quantified using ImageJ. Western blot was performed using HRP-conjugated anti-Fc antibody (Bio-Rad) to additionally analyze and quantify results in ImageJ.

3.2.13. Co-culture experiments and MMRN2 fragment addition experiment

6-well plate that was previously coated with 1% collagen type I (Corning) in 0.1% acetic acid (Carl Roth) for 30 min at room temperature. The plate was washed with PBS (1x; Thermo Fisher Scientific) prior to seeding of MLECs with a density of 1 x 10^5 cells/mL. MLECs at 70% confluence were transfected by using siRNA-mediated knockdown method (Thermo Fisher Scientific) according to the manufacturer's instructions. Next day, MLECs were transfected again. Following day, tumor cells were added onto the endothelial monolayer, and cultured for 4 days. MLECs and tumor cells were

trypsinized using 0.25% Trypsin-EDTA (Thermo Fisher Scientific) for 30 min at 37 °C with 5% CO_2 and recovered with media (DMEM + 10% FBS, L-glutamine (1x); Thermo Fisher Scientific). Samples were subjected to centrifugation for 3 min at 300 x g at room temperature. Supernatant was removed and 500 µL media and 1 µL of DAPI (Thermo Fisher Scientific) were added to each tube. Samples were resuspended and filtered before they were subjected to flow cytometry using BD FACS Melody Cell Sorter (BD Biosciences). MLECs were stained CD31 Pe-Cy7 (Invitrogen) while tumor cells were identified with an mCherry signal and additionally, an mVenus signal if they have become dormant due to the expression of p27. For the protein addition experiment, dormant tumor cells ($CD31^{neg}$ $mCherry^{pos}$ $mVenusp27^{pos}$) from the co-culture were sorted and seeded into 96-well plates. Addition of either 30 $\mu moldm^{-3}$ Fc only, $MMRN2^{(128-487)}$-Fc, $MMRN2^{(487-814)}$-Fc, or PDGFB was done to the sorted dormant tumor cells. Cell count was imaged using the Olympus time-lapse microscope prior to addition of the protein and 36 h post-treatment.

3.2.14. Cryosectioning and immunohistochemistry

Lung samples were subjected to 30% sucrose (Sigma-Aldrich) incubation for 48 h at 4 °C. After dehydration, lungs were transferred to plastic tissue containers, covered with Optimal Cutting Temperature Compound (Tissue-Tek) and put on dry ice until hard. Samples were stored at -20 °C. Lung samples were subjected to cryosectioning using Leica CM3050 S cryostat (Leica Biosystems), providing 30 µm slices that were transferred onto slides. Each slide contained experimental and control group.

Slides containing lung samples were washed two times with PBS (1x; Thermo Fisher Scientific) for 10 min at room temperature in a chamber on a shaker, protected from light. Samples were permeabilized using 0.1% TRITON X-100 (Sigma-Aldrich) for 10 min at room temperature on a shaker. Samples were circled using waterproof marker and subjected to 5% BSA (Biomol) and 0.2% TRITON X-100 (Sigma-Aldrich) blocking solution for 30 min at room temperature in wet chamber, protected from light. Immunostaining was conducted utilizing primary antibodies (dilution 1:50): anti-GFP (Abcam), anti-Ki67 (Invitrogen), and anti-CD31 (Bio-Rad), and incubated overnight at 4 °C in a wet chamber, protected from light. After washing two times with PBS (1x; Thermo Fisher Scientific), bound primary antibodies were detected using fluorophore-conjugated secondary antibodies (dilution 1:300; Invitrogen) for 90 min at room temperature in a wet chamber, protected from light. After washing three times with PBS (1x; Thermo Fisher Scientific), Hoechst (dilution 1:10 000; Thermo Fisher Scientific) was used to label cell nuclei for 15 min at room temperature, protected from light. Samples were washed in PBS (1x; Thermo Fisher Scientific) for 10 min at room temperature on a shaker, protected from light. Samples were mounted using Fluoromount (Merck) and subjected to confocal microscopy using Zeiss Airyscan 880. Images obtained by confocal microscopy were analyzed and quantified using ImageJ.

3.2.15. Primary tumor growth/resection assay

Mice were deeply anaesthetized using 2% isoflurane (Merck). The area in between the rib cage and the left leg was shaved prior to injection of 2.5 x 10^5 B16F10/E0771 tumor cells subcutaneously. Tumor size was checked one week after injection and was monitored for at least 2-3 weeks. Tumor size was calculated with this formula: $\frac{w^2 * l}{2}$, where *w* corresponds to the shorter length of the measurement and *l* corresponds to the longer length. For the resection model, the primary tumor was surgically removed and the wound was sutured using braided polyglycolic acid (PGA) threads (Marlin) while the mice were deeply anaesthetized using 2% isoflurane (Merck). After 6 weeks, the lung was collected and visualized using IVIS (Bio-Rad) as well as immunohistochemistry to identify presence of solitary cells, micrometastasis (2-8 cells), and macrometastasis (>8 cells) alongside their proliferation status using anti-Ki67 antibody (Invitrogen).

3.2.16. Lung metastasis and extravasation assay

Mice were deeply anaesthetized using 2% isoflurane (Merck). The mouse tail was heated with a red lamp to dilate the veins. In a volume of 100 µL, 2.5 x 10^5 B16F10/E0771 tumor cells were injected in the tail vein. Mice were killed one day after injection for the extravasation assay, and 12 days for the lung metastasis assay. For extravasation, lungs were collected and processed for immunohistochemistry. Tumor cells were visualized with GFP antibody (Abcam) and endothelial cells were identified using CD31 staining (Bio-Rad). Tumor cells were counted to have extravasated when it they were outside the vessel in accordance to its location to the endothelial cells. Lung metastasis was quantified using a stereo-microscope (Zeiss) to observe macroscopic metastasis.

3.2.17. Computational prediction analysis

Computational programmes containing human data were used to acquire prediction analysis on how TEM1 and PDGFRB in breast cancer and melanoma affect cancer relapse and survival of patients in remission. Kaplan-Meier Plotter was used to predict probability of cancer relapse various breast cancer subtypes, including ER-positive, PR-positive, HER2-positive, and triple negative. Oncolnc was used to predict survival probability of patients expressing TEM1 and PDGFRB in primary tumors of skin cutaneous melanoma, breast invasive carcinoma, kidney renal papillary carcinoma, bladder urothelial carcinoma, stomach adenocarcinoma, and glioma. Data was analyzed in Prism 9 (GraphPad) for the formation of the survival curve function.

3.2.18. Statistical analysis

In all studies, comparison between mean values was conducted using unpaired, two-tailed parametric/unparametric Student's *t*-test or two-way ANOVA. Pearson correlation was used for analysis

of TEM1 and PDGFRB co-expression assays. Log rank (trend) statistical analysis was used for the survival plots obtained from Oncolnc. In all analyses, statistical significance was determined at the 5% level (*, $p \leq 0.05$; **, $p \leq 0.005$; ***, $p \leq 0.0005$; ****, $p \leq 0.0001$) and mean values ± SEM were described as indicated in the figures. Statistical analysis was performed using Prism 9 (GraphPad) and Excel (Microsoft) to determine if observed differences were statistically relevant.

4. RESULTS

4.1. Lentiviral transduction of *shTEM1* resulted in TEM1 KD in B16F10 melanoma and E0771 breast cancer cells

In order to evaluate the scope of reactivational capacity of upregulated TEM1 in tumor cells, B16F10 melanoma and E0771 breast cancer cell lines containing TEM KD and/or mCherry-Luciferase:mVenus-p27K$^-$ detection system were constructed using lentiviral transduction. Lentiviruses were successfully produced using HEK293T cells and stable constitutive expression of *shScr*, *shTEM1*, *mCherry-Luciferase*, and *mVenus-p27K*$^-$ was achieved. Efficiency of lentiviral transduction targeting TEM1 expression was assessed on a post-transcriptional (mRNA) and post-translational (protein) level, using q-RT-PCR and Western blot, respectively. Western blot displayed a visible reduction in TEM1 protein levels, after the integration of three different types of *shTEM1* (*shTEM-a, shTEM1-b, shTEM1-c*) into the genome, demonstrating that *shTEM1-b* sequence had the most significant impact in reducing TEM1 expression, 72% and 64% in E0771 and B16F10 cells, respectively (Figure 6a,b). q-RT-PCR relative quantification using ΔΔCt method confirmed that in both tumor types, fold change of TEM1 expression was significantly reduced (around 75% for both tumors) after the integration of *shTEM1-b* into the genome (Figure 6c). Thus, *shTEM1-b* was characterized as an effective tool in targeting and promoting TEM1 mRNA degradation, creating stable TEM KD tumor cells lines used throughout the study.

Additionally, TEM1 showed significant increase in its molecular weight after blotting, which corresponds to its high levels of post-translational O-glycosylations. This effect was displayed as a smear on blotting paper containing variable molecular weights, which is consistent with heterogenous glycosylation process in malignant cells. Proteins were therefore subjected to O-glycosidase reaction, which resulted in an increase of one band that represents most stable and common protein state (130 kDa; Figure 6a,b). This common protein variant still had post-translational modifications since its molecular weight was higher than expected 95 kDa of the core protein, suggesting that used O-glycosidase was not able to remove all oligosaccharides.

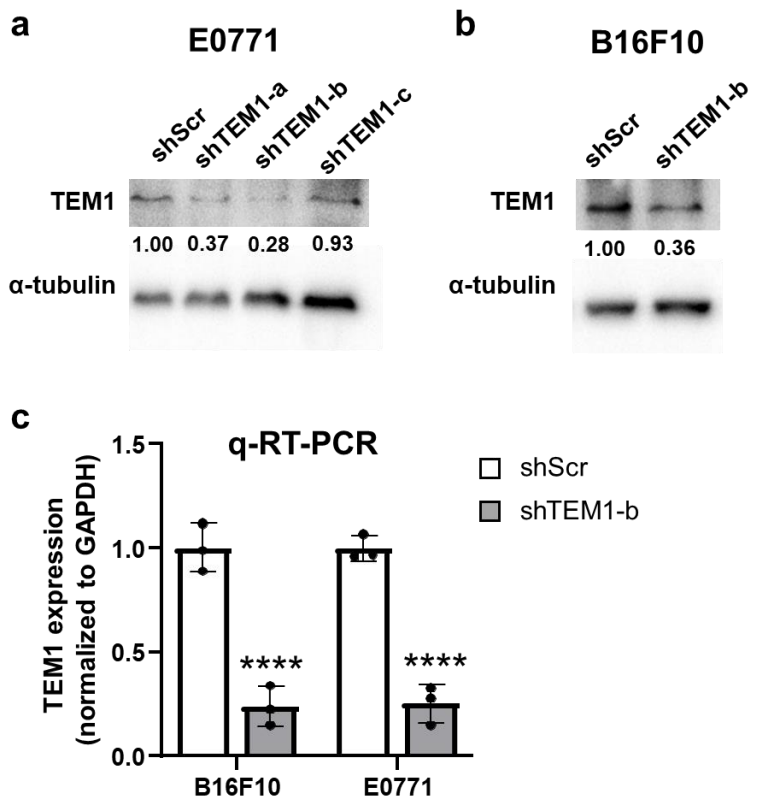

Figure 6. *shTEM1-b* caused knockdown of TEM1 expression in B16F10 and E0771 cells.

(a,b) Images depict relative protein quantification of the reduction of TEM1 expression normalized to α-tubulin after lentiviral transduction of E0771 and B16F10 TCs with *shScr*, *shTEM1-a*, *shTEM1-b*, and *shTEM1-c*. Relative densities were computed using ImageJ. (c) The bar diagram shows relative RNA quantification of TEM1 expression normalized to GAPDH after lentiviral transduction of B16F10 and E0771 TCs with *shTEM1-b*. Ct values were computed using Prism 9 (GraphPad). Data represent mean values ± SEM; ****, $p \leq 0.0001$ (two-tailed parametric Student's *t*-test (c)).

4.2. TEM1 does not affect basal tumor characteristics

In order to assess the functional implications of TEM1 in the proliferative capacity of B16F10 melanoma and E0771 breast cancer, EdU and Ki67 index detection systems were used. Identifying EdU index provided a detailed information about all of the cells that proliferated during the period of nucleotide analog addition, while Ki67 index provided an information on the cells that were proliferating at the end of the assay. For both analyzed tumor types, TEM1 KD did not significantly affect the total number of tumor cells nor the percentage of EdU- and Ki67-positive subpopulation of observed tumor cells (Figure 7a-c; Figure 8a-c).

To investigate the role of TEM1 in uninduced and induced apoptosis of B16F10 melanoma and E0771 breast cancer, tumor cells were subjected to the addition of vehicle and staurosporine, respectively. Cells were sorted into four categories: 1. live non-apoptotic cells, 2. live apoptotic cells, 3. dead apoptotic cells, and 4. dead non-apoptotic cells, using FACS flow cytometry based on their

constitutive GFP fluorescence as well as the addition of annexin V (marker of apoptosis) and 7-AAD (marker of dead cells). In both analyzed tumor types, staurosporine significantly decreased the subpopulation of live cells and subsequently increased the number of apoptotic cells and apoptosis-related dead cells, confirming the apoptotic capacity of stausporine in cell death stimulation (Figure 7d; Figure 8d). TEM1 KD did not have a significant pro- or anti-apoptotic function in both tumor types since the subpopulations in the uninduced and induced sets remained similar, regardless of the existence of TEM1 (Figure 7d; Figure 8d). Slight differences in the cell population distributions could be seen in the induced sets. B16F10 melanoma TEM KD seemed to induce apoptosis more slowly since the subpopulation of dead apoptotic cells was lower, while live non-apoptotic and live apoptotic cells were slightly higher compared to scrambled control (Figure 7d). On the other hand, opposite effect was verified in E0771 breast cancer, where TEM1 KD slightly increased the rate of apoptosis since more dead apoptotic cells and less live apoptotic were detected in comparison to scrambled control (Figure 8d). Generally, the subpopulations affected by apoptosis were not significantly different in the uninduced and induced sets of both tumor types (Figure 7d; Figure 8d).

To assess how TEM1 exerts its migratory function in B16F10 melanoma and E0771 breast cancer, tumor cells were analyzed using scratch wound healing method. TEM1 KD in both tumor types showed no effect in the percentage change of covered area after 16 h (Figure 7e; Figure 8e).

Lastly, to elucidate how TEM1 influences transmigration in B16F10 melanoma and E0771 breast cancer, tumor cells were counted after their migration through the endothelial cell monolayer. Transmigration represents an *in vitro* version of the extravasation process and it showed that TEM1 KD did not significantly affect the number of transmigrated cells in both types of tumor cells (Figure 7f; Figure 8f).

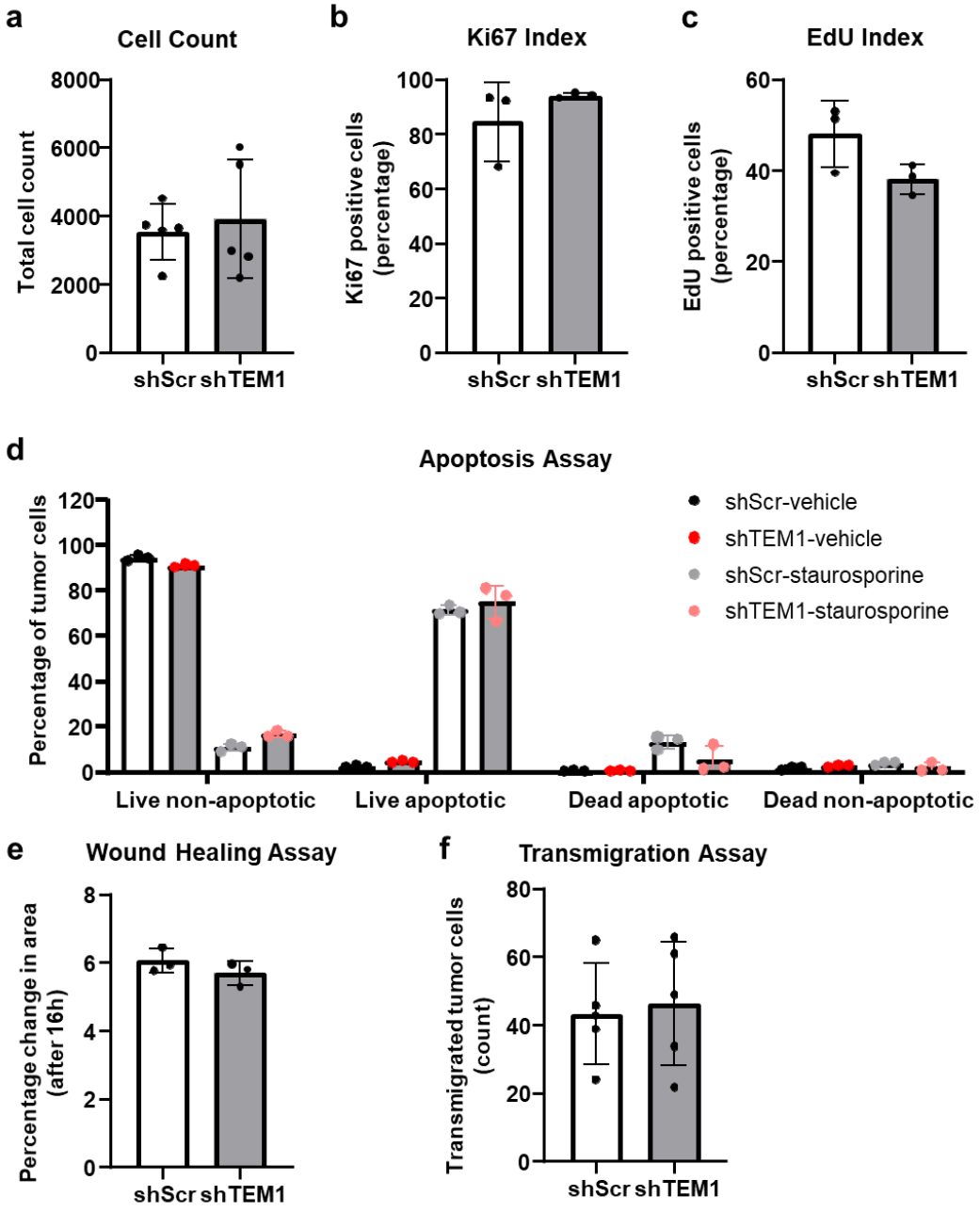

Figure 7. TEM1 knockdown does not affect proliferation, apoptosis, migration, nor transmigration of B16F10 cells.

The bar diagrams depict (a) the total number and percentages of (b) Ki67-positive and (c) EdU-positive TCs 96 h after seeding, (d) percentages of live non-apoptotic, live apoptotic, dead apoptotic, and dead non-apoptotic TCs 6 h after addition of vehicle and staurosporine, (e) percentages of relative area changes 16 h after wound formation, and (f) the total number of transmigrated TCs after 24 h (shScr and shTEM1 B16F10). Data represent mean values ± SEM; (two-tailed parametric Student's *t*-test (a-c,e,f)) and two-way ANOVA (d)).

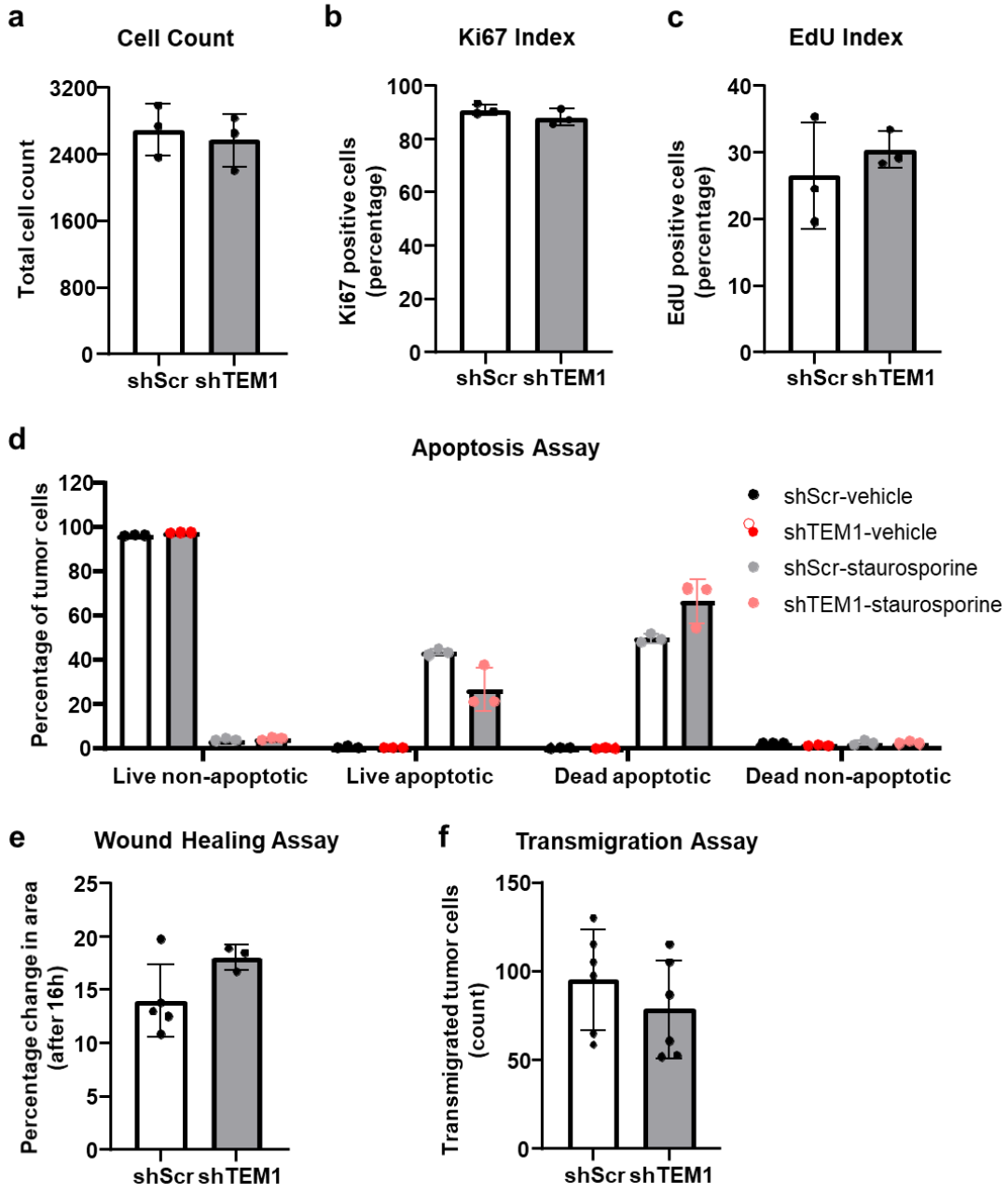

Figure 8. TEM1 knockdown does not affect proliferation, apoptosis, migration, nor transmigration of E0771 cells.

The bar diagrams depict (a) the total number and percentages of (b) Ki67-positive and (c) EdU-positive TCs 96 h after seeding, (d) percentages of live non-apoptotic, live apoptotic, dead apoptotic, and dead non-apoptotic TCs 6 h after addition of vehicle and staurosporine, (e) percentages of relative area changes 16 h after wound formation, and (f) the total number of transmigrated TCs after 24 h (shScr and shTEM1 E0771). Data represent mean values ± SEM; (two-tailed parametric Student's *t*-test (a-c,e,f)) and two-way ANOVA (d)).

4.3. The MMRN2-TEM1 axis increases tumor proliferation

To further investigate how the MMRN2-TEM1 axis influences internal cues governing tumor dormancy and reactivation status, a co-culture system comprised of MLECs and E0771 TEM1 KD was used. Intracellular cues that define proliferation and that were detected using Western blot include total ERK and p-ERK1/2 – a known proliferation marker. Tumor cells cultured alone had significant increase in the total number of tumor cells, regardless of TEM1 status, when compared to the co-culture sets, implicating an endothelium-related dormancy as a potential mechanism of tumor growth reduction (Figure 9a). E0771 breast cancer cells cultured alone showed similar number of tumor cells 4 days post seeding, regardless of the presence of TEM1, which was accompanied by a high p-ERK/total ERK ratio, proving high proliferative capacity of these tumor cells (Figure 9a-c). Tumor cells that were seeded onto scrambled siRNA control endothelial cells showed decrease in the number of tumor cells when TEM1 was not expressed (Figure 9a). Furthermore, E0771 TEM1 KD had low p-ERK/total ERK ratio, indicating low-proliferative capacity (Figure 9b,c). When tumor cells were seeded onto MLECs MMRN2 KD, the amount of tumor cells reduced mostly, compared to the other sets, regardless of the presence of TEM1 (Figure 9a). This result was accompanied by the reduction in p-ERK/total ERK ratio, once again demonstrating low-proliferative capacity (Figure 9b,c). These results were not conducted in triplicates, so statistical significance could not be established. Additionally, B16F10 cell line was ought to be used in this analysis, however Western blot did not show any bands.

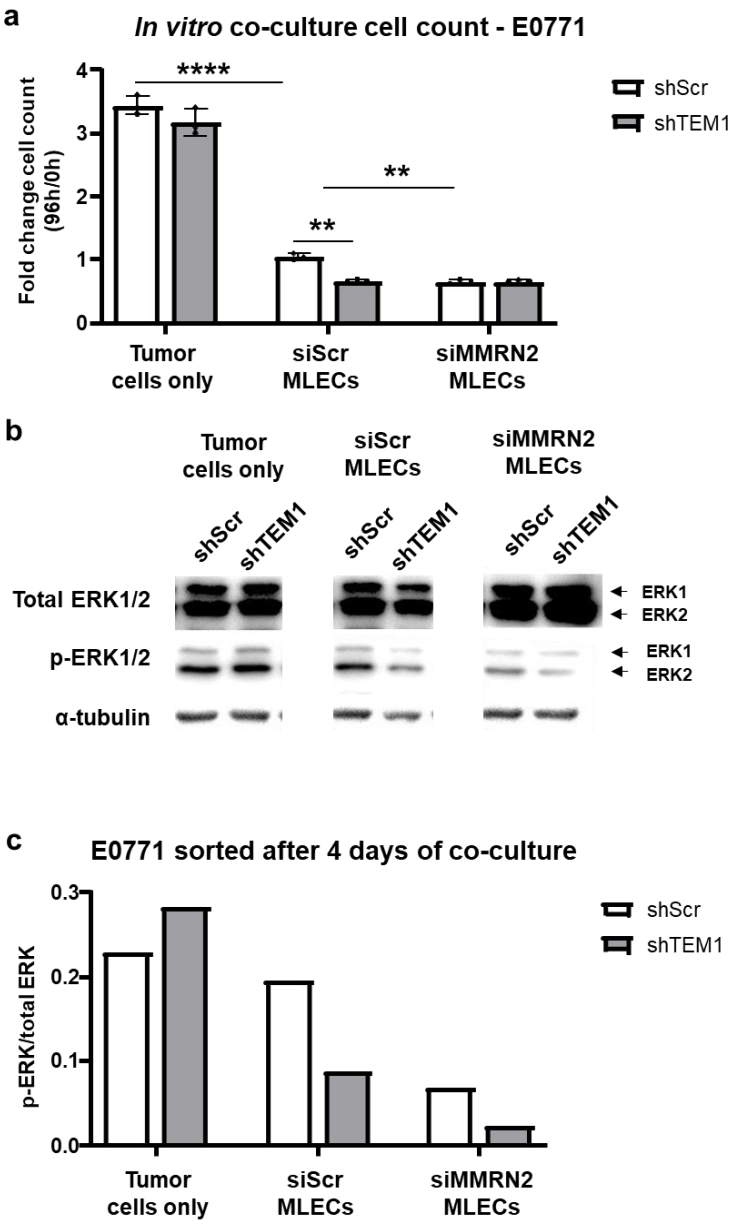

Figure 9. Loss of TEM1 and the MMRN2-TEM1 interaction reduced E0771 proliferative tumor clones and phosphorylated ERK1/2 levels in a co-culture system.

(a) The bar diagrams depict fold change in the total number of TCs 96 h after co-culture with MLECs. (b) Image shows total ERK1/2, p-ERK1/2, and α-tubulin protein expression levels of TCs 4 days after co-culture with MLECs. Relative densities were computed using ImageJ. (c) The bar diagrams show p-ERK/total ERK ratio normalized to α-tubulin in TCs 4 days after co-culture with MLECs (shScr and shTEM1 E0771 – siScr MLECs and siMMRN2 MLECs). Data represent mean values ± SEM; **, $p \leq 0.005$; ****, $p \leq 0.0001$ (two-way ANOVA (a)).

To investigate whether a dormancy is the reason for the observed decrease in the proliferation of tumor cells, a co-culture system comprised of MLECs MMRN2 KD and E0771 TEM KD mCherry:mVenus-p27K$^-$ was established. p27 expression was monitored by the presence of mVenus signal that indicated whether tumor cells had entered a dormant state. FACS flow cytometry delineated

dormant tumor cells from endothelial cells based on their red and green fluorescence ($mCherry^{pos}mVenus^{pos}$; Figure 10a). Tumor cells cultured alone had significantly lower percentages of the cells that were p27-positive, regardless of their TEM1 status, when compared to the co-culture sets, confirming endothelium-related dormancy (Figure 10a,b). Tumor cells that were seeded onto scrambled siRNA control endothelial cells showed significant increase in p27-positive tumor cells when TEM1 was not expressed (Figure 10a,b). When tumor cells were seeded onto MLECs MMRN2 KD, the amount of p27-positive tumor cells increased mostly, compared to the other sets, regardless of the presence of TEM1 (Figure 10a,b). Thus, additive effect of MMRN KD and TEM1 KD in increasing p27 was not confirmed. mCherry:mVenus-$p27K^-$ tumor detection system proved to be an efficient and straightforward tool in assessing proliferation-dormancy status of tumor cells, in comparison to traditional methods of detecting proliferation and dormancy biomarkers using Western blot.

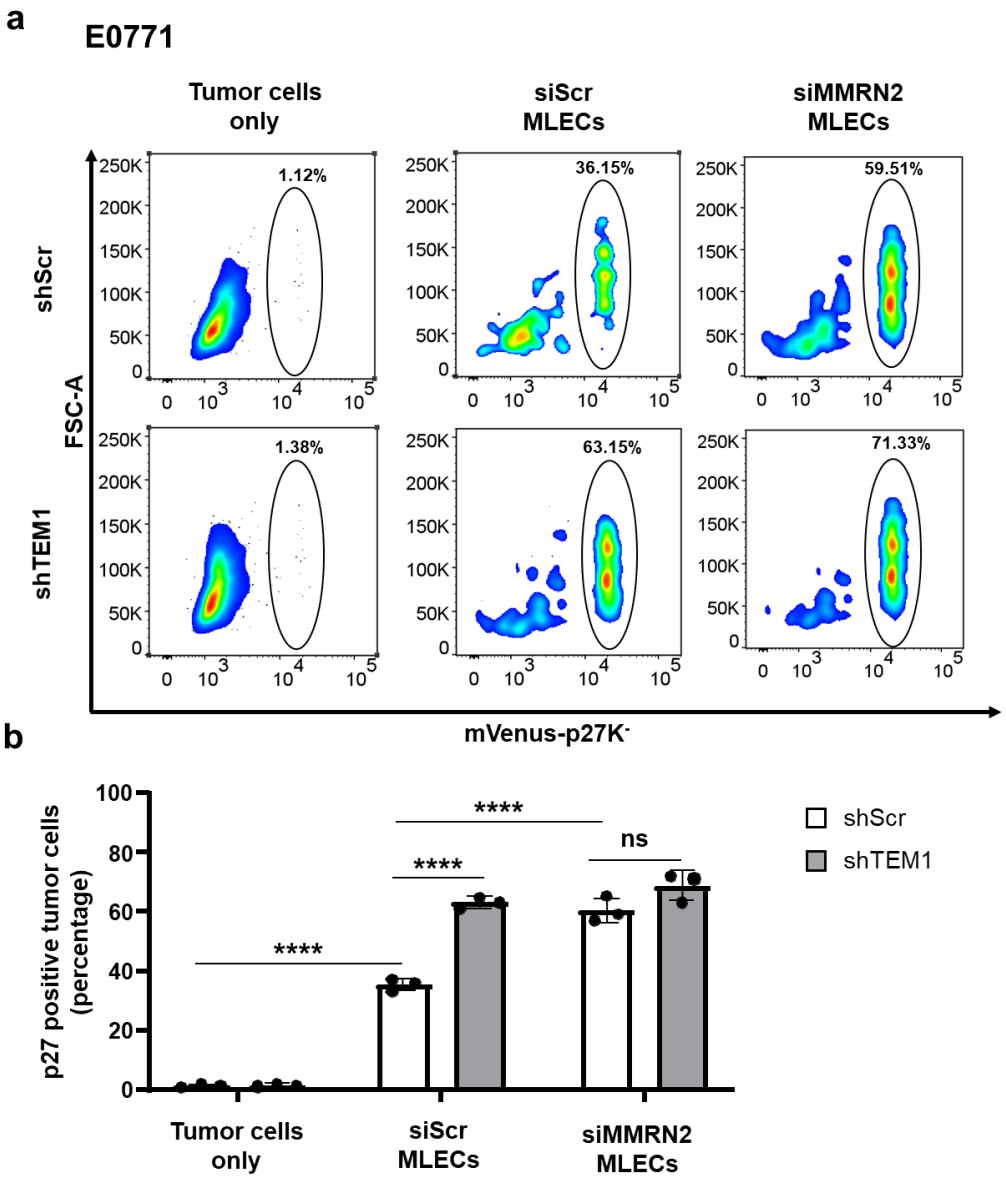

Figure 10. Loss of TEM1 and the MMRN2-TEM1 interaction increased E0771 dormant tumor clones and p27 levels in a co-culture system.

(a) Graph depicts a density plot of dormant TC subpopulation ($CD31^{neg}mCherry^{pos}mVenus^{pos}$) 96 h after co-culture and FACS flow cytometry sorting. (b) The bar diagrams show percentage of p27-positive TCs 96 h after co-culture with MLECs (shScr and shTEM1 E0771 – siScr MLECs and siMMRN2 MLECs). Data represent mean values ± SEM; ****, $p \leq 0.0001$ (two-way ANOVA (b)).

4.4. MMRN2 fragment reactivates tumor cells in a TEM1-dependent manner

In order to test whether dormant tumor cells could be reactivated after a co-culture with endothelial cells, dormant clones were delineated using FACS flow cytometry, based on mCherry:mVenus-p27K^{-} dormancy detection system. CD31^{neg}mCherry^{pos}mVenus^{pos} B16F10 melanoma cells emitting red and green fluorescence, respectively, were sorted for reactivation. Since MMRN2 has a molecular weight of approximately 500 kDa, the protein needed to be expressed and secreted from transfected HEK239T cells as two fragments: MMNR2 fragment 1 (MMRN2$^{(128-487)}$-Fc), which comprises the CC domain of MMRN2 that is known to have TEM1 binding site, and MMRN2 fragment 2 (MMRN2$^{(487-814)}$-Fc; Figure 11a). Recombinant protein fragments were concentrated and isolated, and after SDS-PAGE, Commassie stained gel revealed the presence of Fc, MMRN2 fragment 1 (MMRN2$^{(128-487)}$-Fc), and MMRN2 fragment 2 (MMRN2$^{(487-814)}$-Fc) around 25 kDa, 130 kDa (105 kDa without Fc), and 90 kDa (65 kDa without Fc), respectively, which corresponds with their predicted sizes. In MMRN2$^{(487-814)}$-Fc sample, another band was detected around 35 kDa and it is to be seen to contain an Fc region in the Western blot. Additionally, molar concentrations of Fc, MMRN2$^{(128-487)}$-Fc, and MMRN2$^{(487-814)}$-Fc were estimated using BSA standard curve, showing low concentration levels: 47.17 μmoldm^{-3}, 83.15 nmoldm^{-3}, and 477.78 nmoldm^{-3}, respectively (Figure 11b). In order to confirm concentration efficiency of MMRN2 fragments in the supernatant compared to the cell lysate, Western blot was performed. Fc and MMRN2 fragments were higher after 60x concentration of the supernatant and resembled the results visualized on the gel. Since an unknown fragment at 35 kDa was detected using anti-Fc antibody, it can be assumed that it potentially represents a fragmented protein containing Fc (Figure 11c).

Assessing the role of the MMRN2-TEM1-PDGFRB interaction, addition of Fc, PDGFRB, MMRN2 fragment 1 (MMRN2$^{(128-487)}$-Fc), and MMRN2 fragment 2 (MMRN2$^{(487-814)}$-Fc) onto previously delineated dormant B16F10 melanoma cells revealed significant individual effects of ligands in tumor reactivation (Figure 11d,e). Addition of Fc did not reactivate tumor cells after 36 h between TEM KD and scrambled control. On the other hand, addition of PDGFB caused significant increase of TEM KD tumor cells in comparison to scrambled control. Addition of MMRN2 fragment 1 (MMRN2$^{(128-487)}$-Fc) and MMRN2 fragment 2 (MMRN2$^{(487-814)}$-Fc) showed similar results with significant reduction in reactivated tumor cells with TEM1 KD. This effect was significantly evident after addition of MMRN2 fragment 1 (MMRN2$^{(128-487)}$-Fc) – a polypeptide containing TEM1 binding site, implicating the MMRN2-TEM1 interaction in tumor reactivation capacity. Generally, addition of PDGFRB and MMRN2 fragments significantly increased fold change of the amount of tumor cells in comparison to Fc negative control, demonstrating that Fc does not influence tumor reactivation and proliferation (Figure 11e).

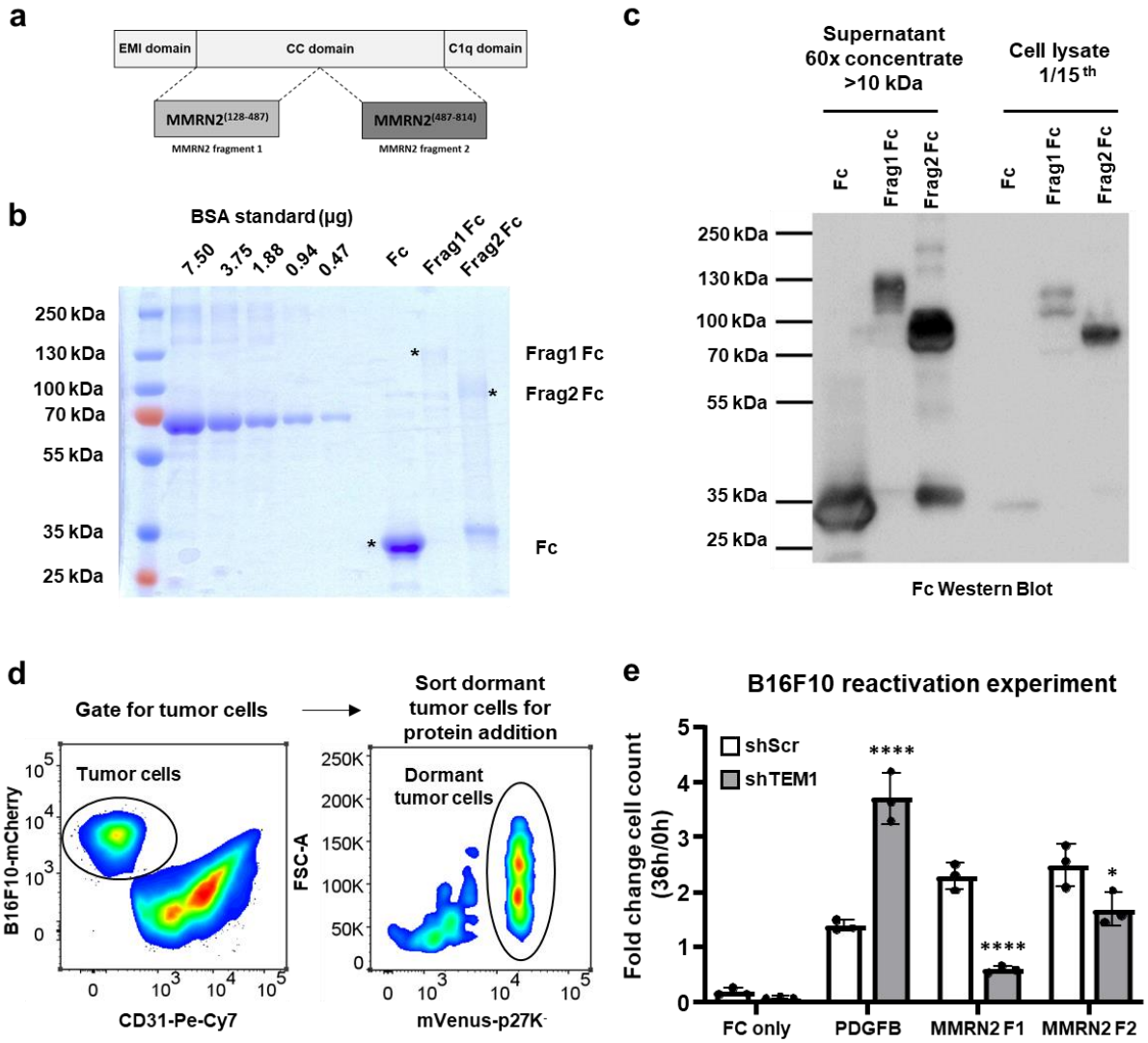

Figure 11. Addition of MMRN2 fragments and PDGFRB reactivated B16F10 dormant TCs. (a) Scheme represents structural domains of MMRN2 (EMI domain, CC domain, and C1q domain) and MMRN2 fragments that were used. (b) Image depicts Coomassie stained gel after SDS-PAGE containing BSA standard concentrations, Fc, MMRN2 fragment 1-Fc, and MMRN2 fragment 2-Fc samples. (c) Image depicts differences in the amount of Fc, MMRN2 fragment 1-Fc, and MMRN2 fragment 2-Fc between supernatant 60x concentrate and cell lysate 1/15th after Western blot. (d) Graphs shows a density plot of the initial total TC population and isolated dormant TC subpopulation (CD31^{neg}mCherry^{pos}mVenus^{pos}) 96 h after co-culture and FACS flow cytometry sorting. (e) The bar diagrams show fold change in the total number of tumor cells 36 h after reactivation with Fc, PDGFB, MMRN2 fragment 1, and MMRN2 fragment 2 (shScr and shTEM1 B16F10). Data represent mean values ± SEM; *, $p \leq 0.05$; ****, $p \leq 0.0001$ (two-way ANOVA (e)).

4.5. TEM1 affects lung metastasis and macrometastasis formation *in vivo*

In order to investigate how TEM1 exerts in functional characteristics in a more clinically-relevant biological settings, rather than in isolated conditions freed of external cues, *in vivo* experiments using mice were done. *In vivo* analysis was conducted using B16F10 melanoma and E0771 breast cancer cell lines to assess comparative relevance of evidence acquired from *in vitro* experiments.

Assessing the functional implications of TEM1 in the process of lung metastasis, B16F10 melanoma and E0771 breast cancer cells were intravenously injected in mice and 14 days post injection visible metastasis present on lung surface were counted. B16F10 and E0771 macrometastasis were both detected on the lungs and the color of metastatic lesions corresponded to their origin and known characteristics, black for melanoma and opaque, whitish color for breast cancer (Figure 12a-c). Both tumor types showed significant decrease in lung metastasis when TEM1 KD was introduced in comparison to the scrambled control (Figure 12a-c).

To understand the role of TEM1 in primary tumor growth, mice were subcutaneously injected with B16F10 melanoma and E0771 breast cancer cells and tumor size was measured until it approximately reached 1 cm^3. Acquired data demonstrated that TEM1 KD in tumor cells did not significantly modulate the rate of primary tumor growth in both tumor types. It is evident that scrambled control and TEM1 KD in B16F10 needed 14 days (Figure 12d), while scrambled control and TEM1 KD in E0771 needed 18 days to reach the size of 1 cm^3 (Figure 12e).

To investigate the role of TEM1 in the extravasation of B16F10 melanoma cells, intravenous injection of tumor cells in mice was performed and lungs sections were analyzed 24 h post injection. Assessment of tumor cells located in blood vessels and those residing in perivascular microenvironment demonstrated that TEM1 KD did not significantly change the percentage of extravasated cells. The average percentage in scrambled control of extravasated cells was around 70%, while that of TEM1 KD was around 72%, showing a slight increase (Figure 12f). In both sets, majority of tumor cells were detected residing in the perivascular space within the capillaries. These observations are consistent with the results obtained from the *in vitro* transmigration assay.

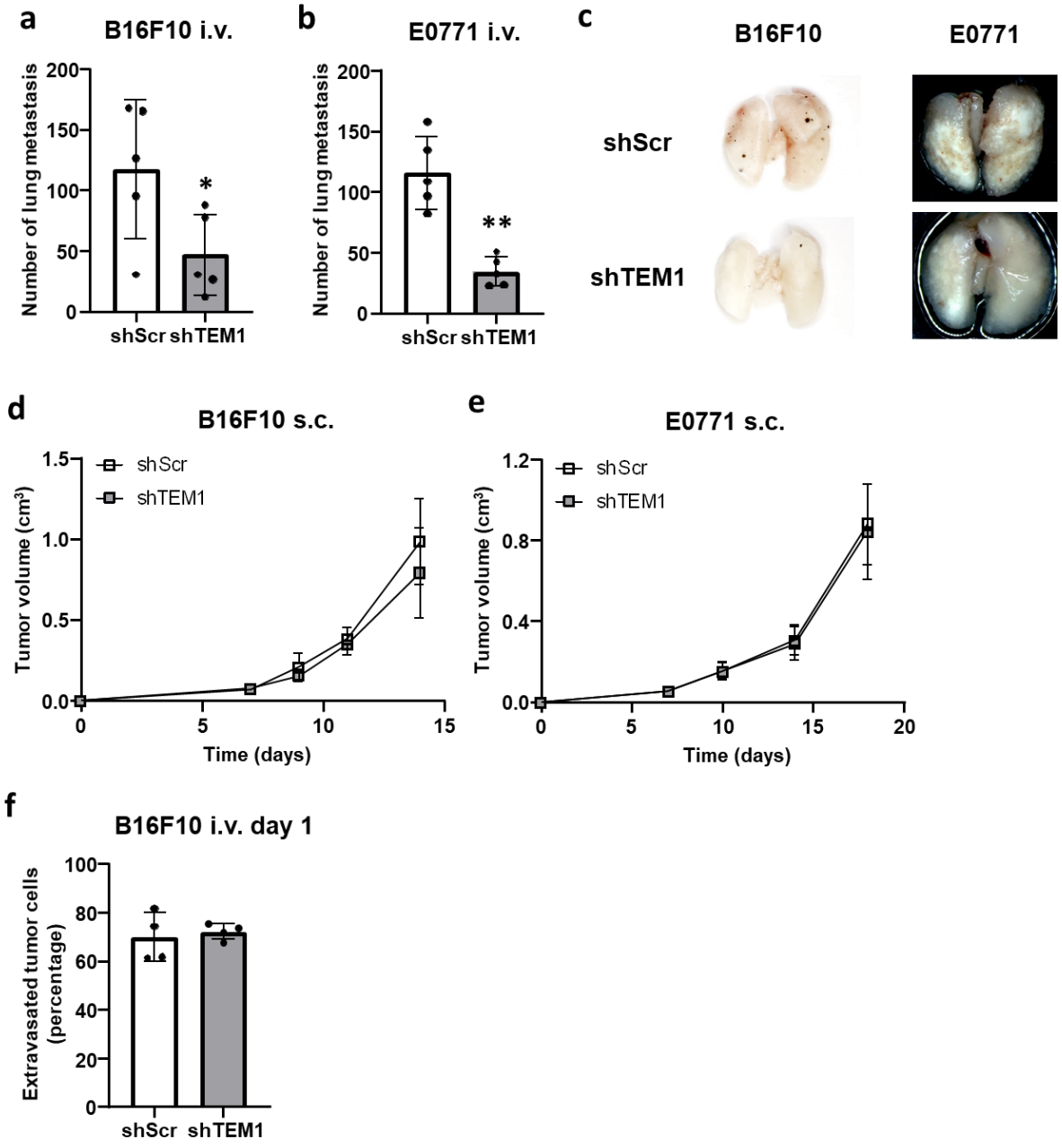

Figure 12. Loss of TEM1 does not affect primary tumor growth in B16F10 and E0771 TCs nor extravasation in B16F10 TCs, but reduces lung metastasis of B16F10 and E0771 TCs *in vivo*. (a) The bar diagram depicts (a) the number of visible lung metastasis using B16F10 TCs and (b) E0771 TCs 12 days post i.v. injection in mice. (c) Image represents lung metastasis of B16F10 TCs and E0771 TCs 12 days post i.v. injection in mice. Graphs show primary tumor growth rate as the dependence of tumor volume (cm^3) per time (days) in (d) B16F10 and in (e) E0771 TCs post s.c. injection in mice. (f) The bar diagram depicts percentage of extravasated B16F10 TCs 24 h post i.v. injection in mice. Data represent mean values ± SEM; *, $p \leq 0.05$; **, $p \leq 0.005$ (two-tailed nonparametric Student's *t*-test (a,b,d-f)).

Additional lung metastasis analysis was conducted using resection model to confirm the role of TEM1 in tumorigenesis, providing a more biological model that incorporates processes such as invasion, intravasation, survival in the circulation, extravasation, and metastatic colonization. Mice were

subcutaneously injected with B16F10 melanoma cells and 6 weeks post resection of the primary tumor, lungs were sectioned and analyzed using immunohistochemistry. All metastatic tumor cells were counted and classified into three groups: 1. solitary cells, 2. micrometastasis (2-8 cells), and 3. macrometastasis (>8 cells), establishing types of metastatic lesions in lungs. TEM1 KD caused loss of radiance after luciferin addition using IVIS, demonstrating the loss of luciferase-expressing tumor cells (Figure 13a). While TEM1 KD did not significantly influence the number of solitary tumor cells and micrometastasis/mm^2, it did show a significant decrease in the number of macrometastasis/mm^2 (Figure 13b,c). More precisely, TEM KD prevented formation of any macrometastasis in analyzed lungs sections under confocal microscopy (Figure 13b). However, general number of macrometastatic lesions was significantly lower than that of micrometastasis and most populous, solitary tumor cells (Figure 13c). Also, it is evident that the distribution of dormant vs proliferative clones in each analyzed group was not significantly different, demonstrating that in the solitary and micrometastatic group most cells were in a dormant state, while in the macrometastatic group, majority of cells were in a proliferative state (Figure 13c).

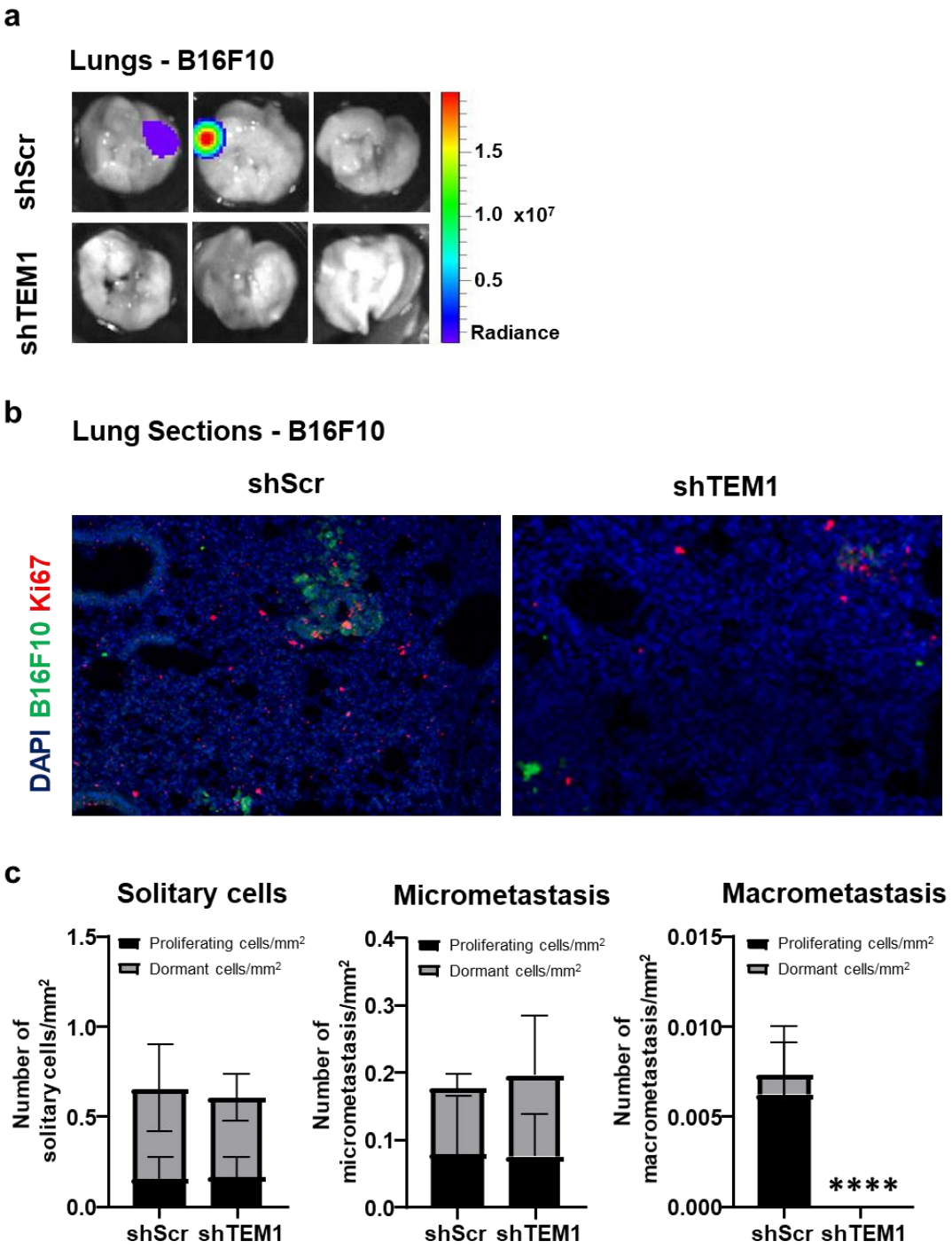

Figure 13. Loss of TEM1 in B16F10 prevented formation of macrometastasis in resection models *in vivo*.

(a) Image depicts measured radiance in (photons/sec) of i.v. injected luciferin marking TCs using IVIS in lungs of tumor-resected mice. (b) Images show lung sections containing macrometastatic lesions of B16F10 TCs using confocal microscopy. Cells were stained with DAPI (blue) and anti-Ki67 antibody (red), and B16F10 TC were visualized through their GFP-expression (green). (c) The bar diagrams depict the total number of solitary cells, micrometastasis (2-8 cells), and macrometastasis (>8 cells) per area (mm^2) as well as subpopulations of proliferative and dormant clones 6 weeks post resection. Data represent mean values ± SEM; ****, $p \leq 0.0001$ (two-tailed nonparametric Student's *t*-test (c)).

4.6. Computational analysis shows that TEM1 and PDGFRB correlate with low overall survival rate and high probability of cancer relapse in various tumor types

In order to foresee the significance of acquired results, implicating TEM1 and PDGFRB in tumor reactivation, comparative analysis involving cancer relapse and survival predictions were performed using commercially available human data programmes – Kaplan-Meier Plotter and Oncolnc. Computational models revealed that expression levels of TEM1 and PDGFRB in various primary tumor types, including skin cutaneous melanoma and breast invasive cancer, were significantly correlated in regards to patients' survival probability (Figure 14a,b). High expressions of both TEM1 and PDGFRB revealed significant decrease in the overall survival rates in skin cutaneous melanoma (Figure 14c), while in breast invasive cancer their uniform upregulation was not significant to be considered as a prognostic marker (Figure 14d). Thus, further analysis of the role of TEM1 and PDGFRB in various breast cancer subtypes, namely ER-positive, PR-positive, HER2-positive, and triple negative breast cancer, demonstrated that only patients with triple negative breast cancer (that corresponds with E0771 used in this study) had higher relapse rates when TEM1 and PDGFRB are highly expressed. All other types of breast cancer patient samples displayed general role of TEM1 and PDGFRB as predictors of good prognosis with decreased level of cancer relapse, implying that prediction values of these proteins vary among breast cancer subtypes (Figure 15). Additionally, high expressions of both TEM1 and PDGFRB displayed significant decrease in the overall survival rates in kidney renal papillary carcinoma (Figure 16a), bladder urothelial carcinoma (Figure 16b), stomach adenocarcinoma (Figure 16c), and glioma (Figure 16d), confirming that similar trends and tight TEM1-PDGFRB correlation is common for many tumor types.

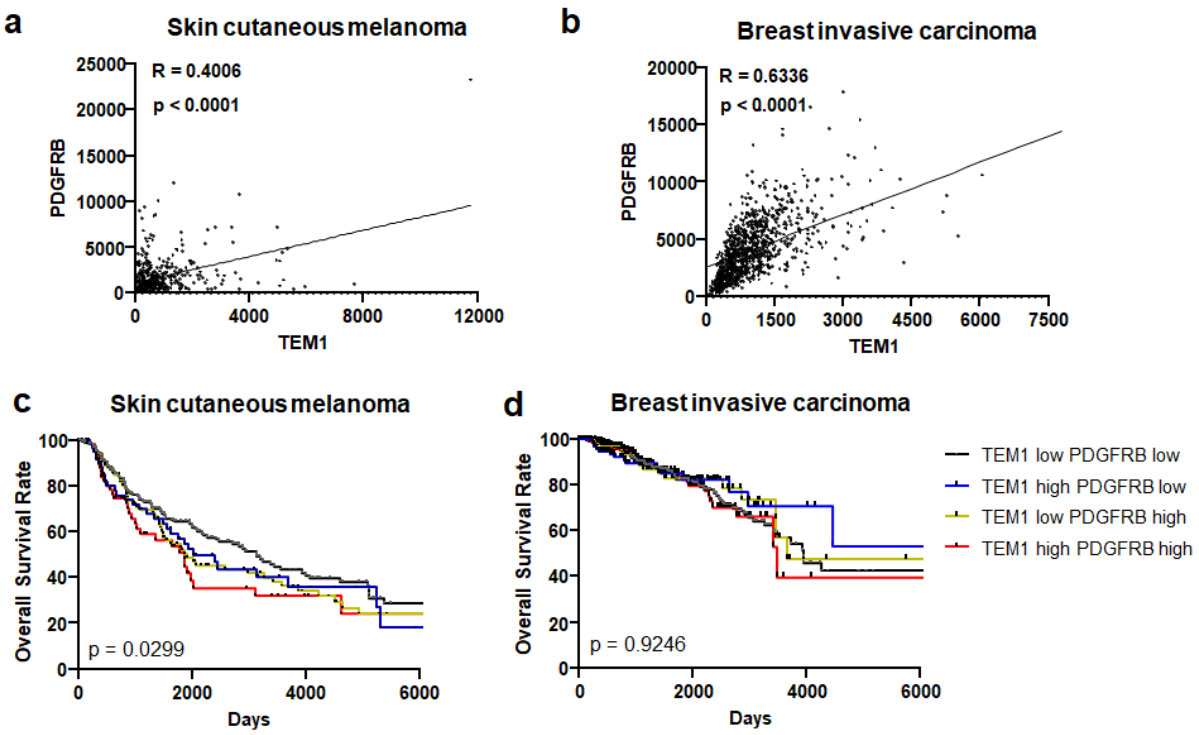

Figure 14. TEM1 and PDGFRB showed high correlation in skin cutaneous melanoma and breast invasive carcinoma, demonstrating low survival rates.

Graphs depict high correlation between TEM1 and PDGFRB in (a) skin cutaneous melanoma and (b) breast invasive carcinoma. Kaplan-Meier graphs show how combinations of TEM1 and PDGFRB expression levels impact the overall survival rate in (c) skin cutaneous melanoma and (d) breast invasive carcinoma. Oncolnc provided human data prediction analysis and Log rank (trend) analysis. Prism 9 (GraphPad) was used for the survival curve analysis. Data represent mean values ± SEM; $p \leq 0.05$ (Pearson correlation (a,b), Log rank (trend) test (c,d)).

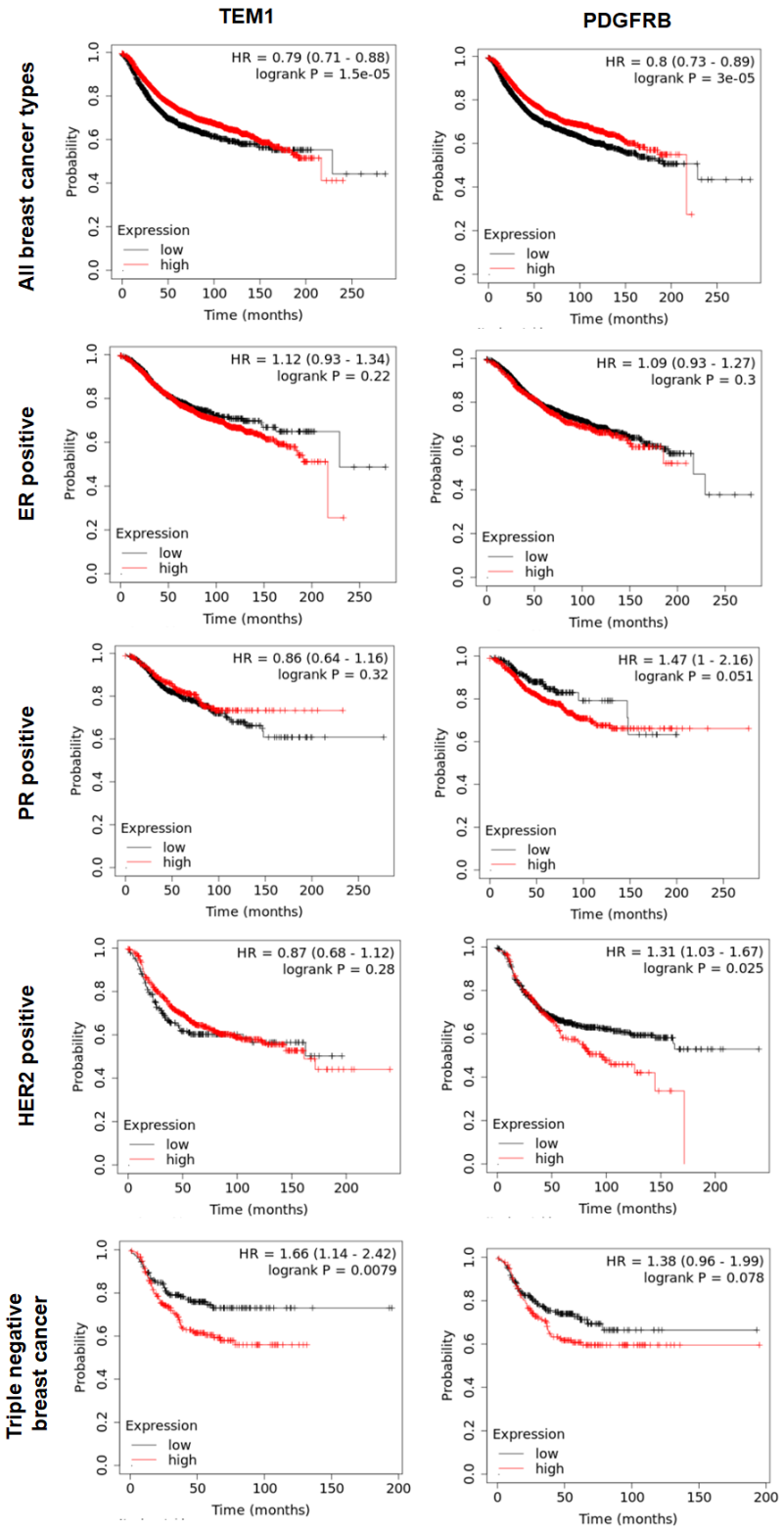

Figure 15. TEM1 and PDGFRB showed high correlation in triple negative breast cancer, demonstrating high possibility of cancer relapse.

Kaplan-Meier graphs show how TEM1 and PDGFRB expression levels impact probability of cancer relapse in all breast cancer types, ER-positive, PR-negative, HER2-negative, and triple negative breast cancer. Kaplan-Meier Plotter provided human data prediction analysis and Log rank (trend) analysis. Data represent mean values ± SEM; $p \leq 0.05$ (Log rank (trend) test).

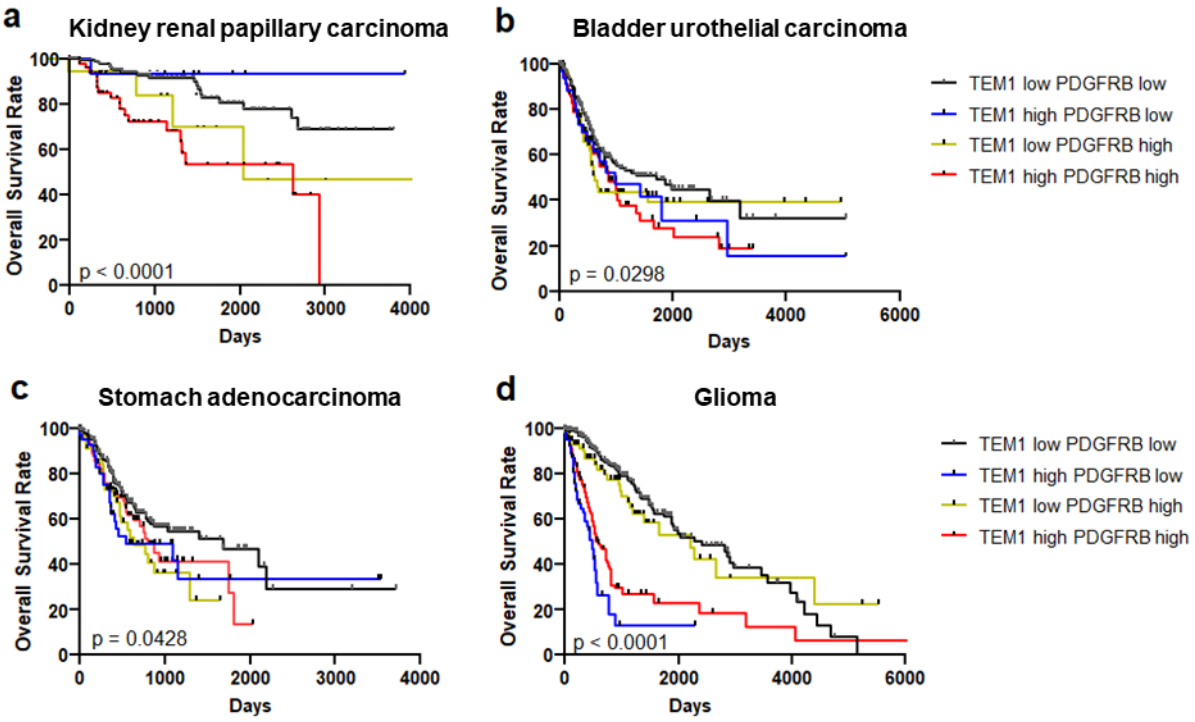

Figure 16. TEM1 and PDGFRB showed high correlation in kidney renal papillary carcinoma, bladder urothelial carcinoma, stomach adenocarcinoma, and glioma.

Kaplan-Meier graphs show how combinations of TEM1 and PDGFRB expression levels impact the overall survival rate in (a) kidney renal papillary carcinoma, (b) bladder urothelial carcinoma, (c) stomach adenocarcinoma, and (d) glioma. Oncolnc provided human data prediction analysis and Log rank (trend) analysis. Prism 9 (GraphPad) was used for the survival curve analysis. Data represent mean values ± SEM; $p \leq 0.05$ (Log rank (trend) test (a-d)).

5. DISCUSSION

Endothelium-derived ligand – MMRN2 has shown its reactivation potential *in vitro* and *in vivo* by promoting lung metastasis and tumorigenesis (Unpublished). To exert its function as an external proliferation-promoting ligand, MMRN2 is hypothesized to act through its known interaction partner – TEM1. MMRN2 is present in the lung perivascular niche in physiological conditions, regardless of the presence of tumors (Christian et al., 2001b; Lorenzon et al., 2012), so it is assumed that tumor cells with proliferating potential and upregulated expression of TEM1 tend to locate near endothelial cells to exhibit the MMRN2-TEM1 interaction, providing proliferative advantage to selected cells prior to metastatic colonization. Upregulated expression levels as well as specific glycosylation patterns of TEM1 in perivascular cells, including pericytes and fibroblasts, have been closely associated with tumorigenesis and angiogenesis (Khan et al., 2017; Noy et al., 2015; Zanivan et al., 2013). However, its structural and functional characteristics in B16F10 melanoma and E0771 breast cancer cells have not been assessed previously.

In this study, MMRN2 KD in endothelial cells and TEM1 KD in tumor cells were used in a co-culture system to analyze the importance of endothelium-tumor axis in dormancy initiation. MMRN2 KD in MLECs and TEM1 KD in tumor cells have individually increased dormancy effect in the co-culture system in terms of cell count and p-ERK/total ERK indexes. These observations have proven that absence of MMRN2 in endothelial cells and TEM1 in tumor cells individually reduce proliferative activity of juxtapositioned tumor cells. mCherry:mVenus-p27K$^-$ detection system has proven to be an effective tool in differentiating dormant clones from proliferating clones, confirming that the reduction in tumor cells is caused by the upregulated activity of p27 – a dormancy biomarker expressed mostly by the cells that exited the cell cycle (Aguirre-Ghiso et al., 2003; Recasens & Munoz, 2019). Additionally, downregulated expression of MMRN2 in endothelial cells reduced proliferative ability of all tumor cells in the co-culture, regardless of the presence of TEM1. This result corroborates not just with the idea that TEM1 expression is required for tumor proliferation (Tomkowicz et al., 2010; Valdez et al., 2012), but also that MMRN2 positively affects proliferative ability of not just pericytes and fibroblasts (Khan et al., 2017; Zanivan et al., 2013), but juxtapositioned tumor cells as well. Thus, the MMRN2-TEM1 interaction is assumed to potentially contribute to overcome the dormancy-inducing function of the endothelium. This interaction however, was not confirmed in this study, providing a possibility for future structural and functional protein-protein interactome evaluations. Individual overexpression of both MMRN2 and TEM1 is recommended to better understand their individual and additive effects in the proliferation axis.

Contrary to the co-culture system results, TEM1 KD in tumor cells cultured alone didn't exhibit any differences in proliferation, apoptosis, migration, nor transmigration. According to the available information regarding interactome and molecular pathway analysis, TEM1 has not been directly

associated with any intracellular proteins involved in the apoptotic signaling pathway. The only implication TEM1 has in cell death is that its overexpression in pericytes can induce apoptosis of juxtapositioned endothelial cells expressing MMRN2 during vascular sprouting in angiogenesis (di Benedetto et al., 2018, 2019), however it remains elusive if this mechanism can be initiated in tumor cells. Thus, evidence presented in this thesis has confirmed that loss of TEM1 does not promote apoptosis of tumor cells, but also does not prevent tumor cells to undergo apoptosis after stimulation with staurosporine. Functional analyses of TEM1 in pericytes and osteosarcoma cells have shown that loss of TEM1 expression has retarded and impaired their proliferative and migratory ability *in vitro* (Tomkowicz et al., 2010; Kondo et al., 2022). However, *in vitro* results using B16F10 melanoma and E0771 breast cancer cell lines have demonstrated that loss of TEM1 in tumor cells does not affect proliferative ability of observed cells. Similarly, no difference in transmigration of B16F10 and E0771 TEM1 KD has been observed. This result is contrary to the osteosarcoma cell experiment that suggests that monoclonal antibody targeting TEM1 suppresses tumor migration through the endothelium, marking TEM1 in fibronectin, and potentially structural factors in the ECM, as crucial cues in transmigration (Kondo et al., 2022). This thesis study has therefore simulated both proliferation and transmigration *in vivo* by subcutaneously and intravenously injecting tumor cells in mice, respectively, and results have shown no changes in the primary tumor growth and the extravasation rates in TEM1 KD tumor cells – similar to the *in vitro* results. However, these results do not exclude that other tumor types (such as osteosarcoma) and/or heterogenous subpopulation of certain tumors may utilize TEM1 in such processes. Even though TEM1 is considered to be upregulated in pathophysiological conditions, its expression levels per cell are still low (unpublished data), potentially explaining once again why loss of already small amount of TEM1 does not impact the proliferation axis more significantly. TEM1 overexpression experiments as well as the usage of a larger pool of tumor types are therefore recommended to better assess the functional impact of TEM1 on tumor cell proliferation and transmigration.

Absence of external cues could be causative of the unchanged proliferative ability in analyzed TEM1 KD tumor cells cultured alone, in contrast to the MLEC-co-culture results and other studies conducted on pericytes (Maia et al., 2011; Tomkowicz et al., 2010), fibroblasts (Christian et al., 2008; Maia et al., 2011), epithelial cells (Brian et al., 2007), and osteosarcoma cells (Kondo et al., 2022). Following this hypothesis, providing MMRN2, a TEM1 ligand, caused reactivation of mVenus-p27K$^-$-positive tumor cells that were sorted from the MLEC-co-culture. Unfortunately, a MMRN2-dependent reactivation of dormant tumor cells could not be achieved using full length MMRN2 since its high molecular weight imposed a problem for efficient protein expression and secretion. That is why MMRN2 was divided into two fragments: MMRN2$^{(128\text{-}487)}$, containing TEM1 binding domain and MMRN2$^{(487\text{-}814)}$, without one. Addition of MMRN2$^{(128\text{-}487)}$ caused reactivation in a TEM1-dependent manner. This result is consistent with previous results of this study in the co-culture experiments, further

implicating that the MMRN2-TEM1 interaction is required for overcoming dormancy induction by the endothelium. Interestingly, addition of MMRN2$^{(487-814)}$ also reactivated mVenus-p27K^{-}-positive tumor cells, albeit in a more TEM1-independent manner, suggesting the existence of other potential binding partners of MMRN2$^{(487-814)}$. Restricted secretion and low efficiency of purification and concentration of MMRN2 fragments prevented additional functional analyses in other tumor cell types (such as E0771 breast cancer) and co-immunoprecipitation experiments to search for other potential MMRN2 binding partners.

The effects of TEM1 KD *in vitro* were translated into *in vivo* settings in order to evaluate the additional roles of external cues present in the perivascular niche that are governing tumor dormancy, and are not present *in vitro*. Thus, the role of TEM1 was set in a biological context that resembles physiological outlook on the metastatic cascade process. Lung metastasis analysis, including intravenous injection of B16F10 melanoma tumor cells and resection model have both shown that tumor cells with TEM1 KD have significantly reduced the number of visible lung metastasis, suggesting that loss of TEM1 reduces proliferative activity that drives metastatic colonization and thus maintains tumor dormancy. Even though TEM1 KD did not influence primary tumor growth, it has significantly reduced the ability of metastatic tumor cells to form visible macrometastasis using both intravenous injection and resection models of lung metastasis. Resection model has provided more physiological results since it was used to simulate the natural process of tumor lung metastasis including invasion, intravasation, survival in the circulation, extravasation, and metastatic colonization. Deciphering comprehensive composition of types of tumor dormancy identified in lungs, it has been revealed that loss of TEM1 did not affect the number of solitary cells and micrometastasis (2-8 cells), but rather caused complete elimination of macrometastasis (>8 cells). This observation could be justified if TEM1 is displayed as a proliferation-supporting factor that exerts its effects in steps following cellular (solitary) tumor reawakening. Concomitantly, TEM1 seems to be closely correlated to mass tumor dormancy, rather than cellular tumor dormancy, since its loss affects only visible and detectable tumor masses. Even though studies have not examined the role of TEM1 in tumor mass dormancy, correlations can be made since absence of TEM1 in perivascular cells has reduced tumor outgrowth, vessel maturation and angiogenesis through modifications in stroma-derived factors (di Benedetto et al., 2019; Khan et al., 2019; Maia et al., 2011). Thus, if this molecular mechanism is to be translated in tumor cells, it can be assumed that deficiency of TEM1 is potentially inclined with the angiogenic type of tumor mass dormancy since changes in its expression could have opposite effects on dormancy-reactivation balance. Elucidation of molecular mechanisms on how stimulated changes of expression impact cellular/micrometastatic-macrometastatic shift as well as angiogenic relevance to tumor mass dormancy should all be validated. Additionally, TEM1 overexpression experiments and increasing tumor cell types for analysis could further implicate whether the observed mechanisms apply to majority of tumor types. Also,

mCherry:mVenus-p27K^{-} detection system should be considered to be utilized in *in vivo* research for easier and more straightforward differentiation of dormant clones from proliferative ones in lung tissues.

Observed proliferative defects of TEM1 KD tumor cells *in vitro* and *in vivo* were further investigated by checking levels of p27 and p-ERK1/2. A co-culture system containing MLECs and E0771 breast cancer cells has confirmed previously described results and revealed that loss of TEM1 in tumor cells has reduced the ratio of p-ERK/total ERK and concurrently increased p27. Thus, detected p-ERK^{low}/p27^{high} expression profile reflects dormancy status of the cells that lack TEM1, confirming that the reason for the reduction in the total number of tumor cells without TEM1 after culturing onto functional endothelial cells is correlated with simultaneous increase of tumor dormancy. Thus, TEM1 seems to be implicated in positive modulation of ERK1/2 and promote p-ERK^{high}/p27^{low} proliferative status of tumor cells. On the other hand, culturing tumor cells onto MLECs with inhibited MMRN2 expression has caused reduced ratio of p-ERK/total ERK, regardless of the presence of TEM1, and high increase of p27. Additionally, additive effect of MMRN2 KD and TEM1 KD could be seen in p-ERK1/2 expression levels. These observations reflect the previously stated thesis that juxtaposition of endothelial cells and tumor cells is necessary for MMRN2 deposits to potentially activate TEM1 and thus promote proliferation. Tumor cells cultured alone have confirmed their increased proliferating activity with highest p-ERK^{high}/p27^{low} status since these cells are not affected by potential restraining signals from endothelial cells and utilize various proliferating signaling pathways that do not depend solely on TEM1. Significance of these differences needs to be examined further by repeating molecular analysis of dormancy-reactivation status since statistical relevance was not able to be conducted. Additionally, p-p38 is recommended to be detected since the ratio p-ERK^{low}/p-p38^{high} represents a more acceptable and commonly used measure of tumor dormancy (Aguirre-Ghiso et al., 2003; Recasens & Munoz, 2019).

Deciphering the potential signaling cascade of MMRN2-TEM1 to promote tumor reactivation *in vitro* and *in vivo* can further fine-tune potential therapeutic approaches to treat minimal residual disease. As this study has shown that TEM1 signals through p-ERK1/2, it was therefore investigated whether the effects observed are through its potential co-receptor PDGFRB. This thesis has confirmed that dormant B16F10 melanoma cells can be reactivated by PDGFB addition, which coincides with the proliferation activity of the PDGFRB pathway (Valdez et al., 2012). However, loss of TEM1 in PDGFB-reactivated tumor cells has shown significantly higher proliferative ability than the ones with TEM1, which seems contradictory to the previously proposed mechanism. Since those results cannot be explained, repeating PDGFB addition should be considered. Reactivation experiments should also be done in PDGFRB KD cells to see whether the effects of MMRN2 are both in a TEM1- and PDGFRB-dependent manner. Future prospects for elucidating the MMRN2-TEM1-PDGFRB signaling axis should also focus on different combinations of PDGFB, MMRN2$^{(128-487)}$, and MMRN2$^{(487-814)}$ to emphasize their potential additive effects *in vitro* co-culture systems and *in vivo* intravenous injection and resection models of lung metastasis. Moreover, antibodies targeting PDGFRB, MMRN2$^{(128-487)}$, and MMRN2$^{(487-}$

[814] could be used in the same types of experiments, emphasizing a more pharmacological application to potentially target reactivation-related molecular mechanisms without side effects in normal biological processes. Defining the exact molecular concentrations of PDGFB and MMRN2 and their post-translational modifications present in the lung perivascular niche could also provide an additional physiological outlook on the amount of ligands necessary for TEM1-induced tumor reactivation. Finally, elucidating molecular cues and conditions that upregulate TEM1 expression can shed a light on other approaches to further inhibit tumor reactivation.

In vitro and *in vivo* models of tumor dormancy and reactivation have shown that tumor cells with low TEM1 expression levels have impaired proliferative capacity for macrometastasis formation. The overall survival rates based on the computational human patient data models have implicated that primary tumors having high expression levels of both TEM1 and PDGFRB can act as a prognostic marker for several cancer types. In particular, skin cutaneous melanoma, kidney renal papillary carcinoma, bladder urothelial carcinoma, stomach adenocarcinoma, and glioma have all revealed high expression levels of TEM1 and PDGFRB which led to poor patient outcomes. Significant correlation of TEM1 and PDGFRB expression found in various tumor types supports the notion that these proteins and their molecular functions overlap and mutually affect tumorigenesis. This was evident in the decreased overall survival rates of patients with high expression levels of both TEM1 and PDGFRB. Even though these observations from patients relate to tumorigenic functions of TEM1 and PDGFRB in primary tumors, their effect in cancer relapse at secondary sites remains unclear. Correlation of high TEM1 and PDGFRB expression in breast invasive cancer at primary site has not shown significant decrease in the overall survival rate to be used as a prognostic marker. However, high TEM1 and PDGFRB expression in triple negative breast cancer, which is analogous to E0771 breast cancer used in this study, has resulted in a significant increase in possibility of cancer relapse which coincides with the proposed thesis that TEM1 and PDGFRB promote tumor reactivation and metastatic outgrowth in a similar manner as they do in stromal cells (Tomkowicz et al., 2010). Other breast cancer subtypes have revealed variable impacts of TEM1 and PDGFRB as cancer relapse predictors, implying that the role of these reactivation factors is cell-specific. Limitations regarding clinical relevance of human data prediction models that could be used as prognostic markers is due to the lack of single-cell resolution methods that would distinguish whether the low survival and the increased probability to exert cancer relapse effects of TEM1 and PDGFRB comes directly from tumor cells or stromal cells, since they both express these proteins that positively influence tumorigenesis. Thus, future prospects rely on addressing potential additive effects of upregulated TEM1 in tumor cells and surrounding tissues in tumor promotion, with a key focus in determining the exact contribution of each TEM1 expressing cell type in tumor reactivation and proliferation.

As maintenance and exit from tumor cell dormancy relies on a specific set of extracellular cues that differ from one organ-specific milieu to another and varies among patients (Summers et al., 2020;

Yeh & Ramaswamy, 2015), a more personalized approach in treating minimal residual disease is becoming more apparent. Efficiency of treatment therefore depends whether the dormancy/reactivation pathway being targeted is highly represented in the cancer cells. As it is shown that patients with high TEM1 and PDGFRB expression have higher probability of cancer relapse, they will potentially benefit more from drugs that inhibit their signaling more than those who have low expression levels of both TEM1 and PDGFRB. Thus, patients in remission diagnosed with skin cutaneous melanoma, triple negative breast cancer, kidney renal papillary carcinoma, bladder urothelial carcinoma, stomach adenocarcinoma, and high-grade glioma could be good responders for TEM1/PDGFRB blockers in suppressing cancer relapse if these molecules are overrepresented in their primary tumors. Among innovative therapeutic platforms targeting TEM1, Ontuxizumab is currently the only emerging adjuvant that is undergoing clinical trials and showing promise in monoclonal antibody-based therapies, acting as an inhibitor of cancer relapse (Creative Biolabs, Recombinant antibody 2022). While treatment responders enable development of TEM1 inhibitors that can successfully prevent tumor recurrence, being beneficial for patients in remission, development of potential activators of TEM1 could also be vital to purposely stimulate tumor growth which can be intended to patients undergoing operation or patients on anti-proliferative treatments (chemotherapy and/or radiotherapy). Since there is an increasing number of emerging dormancy and reactivation cues, similar investigations can provide larger pool of prognostic factors and thus adequate therapeutic approaches can be taken in order to prevent poor patient outcomes. All things considered, this study represents a pioneering research in investigating integrated roles of MMRN2, TEM1, and PDGFRB in tumor progression. Acquired new revelations pose a basis for development of innovative, state-of-the-art, personalized therapies that intend to inhibit reactivation of dormant tumor cells in patients considered to be or undergoing cancer relapse.

6. CONCLUSIONS

This study has established tumor endothelial marker 1 (TEM1) as a potential tumor reactivation/proliferation molecule in B16F10 melanoma and E0771 breast cancer metastatic clones. Absence of either TEM1 in tumor cells or MMRN2 in endothelial cells both decreased tumor proliferation in *in vitro* co-culture systems and promoted tumor mass dormancy in *in vivo* lung metastasis models. The phenotypic observations in the knockdown experiments performed were due to the decreased Ki67 protein levels and phosphorylation of ERK1/2, while increasing p27 protein abundance in tumor cells. $MMRN2^{(128-487)}$, a fragment which contains TEM1 binding site, promoted reactivation of dormant tumor cells in a TEM1-dependent manner, confirming the necessity of both, a ligand and a receptor molecule to initiate tumor proliferation. As PDGFB has also been shown to be a potential reactivator, future experiments can focus on investigating whether the coordination between the PDGFB-PDGFRB and MMRN2-TEM1 axes in pericyte proliferation will be recapitulated in the observed TEM1-induced tumor reactivation, particularly with TEM1 acting as a co-receptor/enhancer of the PDGFB/PDGFRB signaling axis. According to available human data, TEM1 and PDGFRB appear to be prediction markers of poor prognosis as their correlated upregulated expression has led to lower overall survival rates and higher relapse rates in various tumor types. This thesis thus represents a pioneering research in understanding the MMRN2-TEM1 axis in tumor reactivation and poses a basis for developing personalized pharmacological therapeutics that would treat patients in remission by either helping eradicate all indolent tumor cells or maintaining their quiescence, thereby reducing high mortality rates triggered by cancer relapse.

7. REFERENCES

Agarwal, P., Isringhausen, S., Li, H., Paterson, A. J., He, J., Gomariz, Á., Nagasawa, T., Nombela-Arrieta, C., & Bhatia, R. (2019): Mesenchymal niche-specific expression of CXCL12 controls quiescence of treatment-resistant leukemia stem cells. Cell Stem Cell 24(5): 769-784.e6.

Aguirre-Ghiso, J. A., Estrada, Y., Liu, D., & Ossowski, L. (2003): ERK (MAPK) activity as a determinant of tumor growth and dormancy; regulation by p38 (SAPK 1). Cancer Research 63(7): 1684-1695.

Albrengues, J., Shields, M. A., Ng, D., Park, C. G., Ambrico, A., Poindexter, M. E., Upadhyay, P., Uyeminami, D. L., Pommier, A., Küttner, V., Bružas, E., Maiorino, L., Bautista, C., Carmona, E. M., Gimotty, P. A., Fearon, D. T., Chang, K., Lyons, S. K., Pinkerton, K. E., … Egeblad, M. (2018): Neutrophil extracellular traps produced during inflammation awaken dormant cancer cells in mice. Science 361(6409): eaao4227.

Almog, N. (2010): Molecular mechanisms underlying tumor dormancy. Cancer Letters 294(2): 139-146.

Brian, T., Katherine, R., Brian, F., Wolfgang, E., Brad, K., Eric, R., Philip, S., C, N. N., Luigi, G., & Yuhong, Z. (2007): Interaction of endosialin/TEM1 with extracellular matrix proteins mediates cell adhesion and migration. Proceedings of the National Academy of Sciences of the United States of America 104(46): 17965-17970.

Cesinaro, A. M., Natoli, C., Grassadonia, A., Tinari, N., Iacobelli, S., & Trentini, G. P. (2002): Expression of the 90K tumor-associated protein in benign and malignant melanocytic lesions. The Journal of Investigative Dermatology, 119(1): 187-190.

Christian, S., Ahorn, H., Koehler, A., Eisenhaber, F., Rodi, H. P., Garin-Chesa, P., Park, J. E., Rettig, W. J., & Lenter, M. C. (2001a): Molecular cloning and characterization of endosialin, a C-type lectin-like cell surface receptor of tumor endothelium. The Journal of Biological Chemistry 276(10): 7408-7414.

Christian, S., Ahorn, H., Novatchkoval, M., Garin-Chesa, P., Park, J. E., Weber, G., Eisenhaber, F., Rettig, W. J., & Lenter, M. C. (2001b): Molecular cloning and characterization of EndoGlyx-1, an EMILIN-like multisubunit glycoprotein of vascular endothelium. The Journal of Biological Chemistry 276(51): 48588-48595.

Christian, S., Winkler, R., Helfrich, I., Boos, A. M., Besemfelder, E., Schadendorf, D., & Augustin, H. G. (2008): Endosialin (Tem1) is a marker of tumor-associated myofibroblasts and tumor vessel-associated mural cells. The American Journal of Pathology 172(2): 486-494.

Colladel, R., Pellicani, R., Andreuzzi, E., Paulitti, A., Tarticchio, G., Todaro, F., Colombatti, A., & Mongiat, M. (2016): MULTIMERIN2 binds VEGF-A primarily via the carbohydrate chains exerting an angiostatic function and impairing tumor growth. Oncotarget 7(2): 2022-2037.

Coller, H. A., Sang, L., & Roberts, J. M. (2006): A new description of cellular quiescence. PLoS Biology 4(3): e83.

Colombatti, A., Spessotto, P., Doliana, R., Mongiat, M., Bressan, G. M., & Esposito, G. (2012): The EMILIN/multimerin family. Frontiers in Immunology 2: 93.

Damen, M. P. F., van Rheenen, J., & Scheele, C. L. G. J. (2021): Targeting dormant tumor cells to prevent cancer recurrence. The FEBS Journal 288(21): 6286-6303.

di Benedetto, P., Liakouli, V., Ruscitti, P., Berardicurti, O., Carubbi, F., Panzera, N., di Bartolomeo, S., Guggino, G., Ciccia, F., Triolo, G., Cipriani, P., & Giacomelli, R. (2018): Blocking CD248 molecules in perivascular stromal cells of patients with systemic sclerosis strongly inhibits their differentiation toward myofibroblasts and proliferation: A new potential target for antifibrotic therapy. Arthritis Research & Therapy 20(1): 223.

di Benedetto, P., Ruscitti, P., Liakouli, V., del Galdo, F., Giacomelli, R., & Cipriani, P. (2019): Linking myofibroblast generation and microvascular alteration: The role of CD248 from pathogenesis to therapeutic target (Review). Molecular Medicine Reports 20(2): 1488-1498.

Di, J., Sinai, M. M., Nobre, A. R., Mondal, C., Farias, E., Fertig, E., Naba, A., Aguirre-Ghiso, J., & Bravo-Cordero, J. J. (2021): A tumor-derived type III collagen-rich ECM niche regulates tumor cell dormancy. Nature Cancer 3(1): 90-107.

Dunn, G. P., Old, L. J., & Schreiber, R. D. (2004): The immunobiology of cancer immunosurveillance and immunoediting. Immunity 21(2): 137-148.

Egeblad, M., Nakasone, E. S., & Werb, Z. (2010): Tumors as organs: complex tissues that interface with the entire organism. Developmental Cell 18(6): 884-901.

Er, E. E., Valiente, M., Ganesh, K., Zou, Y., Agrawal, S., Hu, J., Griscom, B., Rosenblum, M., Boire, A., Brogi, E., Giancotti, F. G., Schachner, M., Malladi, S., & Massagué, J. (2018): Pericyte-like spreading by disseminated cancer cells activates YAP and MRTF for metastatic colonization. Nature Cell Biology 20(8): 966-978.

Eyles, J., Puaux, A. L., Wang, X., Toh, B., Prakash, C., Hong, M., Tan, T. G., Zheng, L., Ong, L. C., Jin, Y., Kato, M., Prévost-Blondel, A., Chow, P., Yang, H., & Abastado, J. P. (2010): Tumor cells disseminate early, but immunosurveillance limits metastatic outgrowth, in a mouse model of melanoma. The Journal of Clinical Investigation 120(6): 2030-2039.

Fares, J., Fares, M. Y., Khachfe, H. H., Salhab, H. A., & Fares, Y. (2020): Molecular principles of metastasis: a hallmark of cancer revisited. Signal Transduction and Targeted Therapy 5(1): 28.

Gao, H., Chakraborty, G., Lee-Lim, A. P., Mo, Q., Decker, M., Vonica, A., Shen, R., Brogi, E., Brivanlou, A. H., & Giancotti, F. G. (2012): The BMP inhibitor Coco reactivates breast cancer cells at lung metastatic sites. Cell 150(4): 764-779.

Gao, X. L., Zhang, M., Tang, Y. L., & Liang, X. H. (2017): Cancer cell dormancy: mechanisms and implications of cancer recurrence and metastasis. OncoTargets and Therapy 10: 5219-5228.

Gawrzak, S., Rinaldi, L., Gregorio, S., Arenas, E. J., Salvador, F., Urosevic, J., Figueras-Puig, C., Rojo, F., del Barco Barrantes, I., Cejalvo, J. M., Palafox, M., Guiu, M., Berenguer-Llergo, A., Symeonidi, A., Bellmunt, A., Kalafatovic, D., Arnal-Estapé, A., Fernández, E., Müllauer, B., … Gomis, R. R. (2018): MSK1 regulates luminal cell differentiation and metastatic dormancy in ER+ breast cancer. Nature Cell Biology 20(2): 211-221.

Ghajar, C. M. (2015): Metastasis prevention by targeting the dormant niche. Nature Reviews Cancer 15(4): 238-247.

Ghajar, C. M., Peinado, H., Mori, H., Matei, I. R., Evason, K. J., Brazier, H., Almeida, D., Koller, A., Hajjar, K. A., Stainier, D. Y. R., Chen, E. I., Lyden, D., & Bissell, M. J. (2013): The perivascular niche regulates breast tumour dormancy. Nature Cell Biology 15(7): 807-817.

Gomis, R. R., & Gawrzak, S. (2017): Tumor cell dormancy. Molecular Oncology 11(1): 62-78.

Hanahan, D., & Weinberg, R. A. (2011): Hallmarks of cancer: the next generation. Cell 144(5): 646-674.

Holmgren, L., & Folkman, U. (1995): Dormancy of micrometastases: balanced proliferation and apoptosis in the presence of angiogenesis suppression. Nature Medicine 1(2): 149-153.

Indraccolo, S., Favaro, E., & Amadori, A. (2006a): Dormant tumors awaken by a short-term angiogenic burst: the spike hypothesis. Cell Cycle 5(16): 1751-1755.

Indraccolo, S., Stievano, L., Minuzzo, S., Tosello, V., Esposito, G., Piovan, E., Zamarchi, R., Chieco-Bianchi, L., & Amadori, A. (2006b): Interruption of tumor dormancy by a transient angiogenic burst within the tumor microenvironment. Proceedings of the National Academy of Sciences of the United States of America 103(11): 4216-4221.

Khan, K. A., McMurray, J. L., Mohammed, F., & Bicknell, R. (2019): C-type lectin domain group 14 proteins in vascular biology, cancer and inflammation. The FEBS Journal 286(17): 3299-3332.

Khan, K. A., Naylor, A. J., Khan, A., Noy, P. J., Mambretti, M., Lodhia, P., Athwal, J., Korzystka, A., Buckley, C. D., Willcox, B. E., Mohammed, F., & Bicknell, R. (2017): Multimerin-2 is a ligand for group 14 family C-type lectins CLEC14A, CD93 and CD248 spanning the endothelial pericyte interface. Oncogene 36(44): 6097-6108.

Kondo, Y., Honoki, K., Kishi, S., Mori, S., Fujiwara-Tani, R., Tsukamoto, S., Fujii, H., Kuniyasu, H., & Tanaka, Y. (2022): Endosialin/CD248 may be a potential therapeutic target to prevent the invasion and metastasis in osteosarcoma. Oncology Letters 23(2): 42.

Langley, R. R., & Fidler, I. J. (2011): The seed and soil hypothesis revisited – the role of tumor-stroma interactions in metastasis to different organs. International Journal of Cancer 128(11): 2527-2535.

Lavoie, J. N., L'Allemain, G., Brunei, A., Müller, R., & Pouysségur, J. (1996): Cyclin D1 expression is regulated positively by the p42/p44MAPK and negatively by the p38/HOGMAPK pathway. The Journal of Biological Chemistry 271(34): 20608-20616.

Liu, S., Xu, C., Zhang, K., Han, D., Yang, F., Li, Y., Zhao, X., Ma, S., Li, H., Lu, S., Lu, T., Zhang, J., Qin, W., Wen, W., & Yang, B. (2021): CD248 as a bridge between angiogenesis and immunosuppression: a promising prognostic and therapeutic target for renal cell carcinoma. Annals of Translational Medicine 9(23): 1741.

Lorenzon, E., Colladel, R., Andreuzzi, E., Marastoni, S., Todaro, F., Schiappacassi, M., Ligresti, G., Colombatti, A., & Mongiat, M. (2012): MULTIMERIN2 impairs tumor angiogenesis and growth by interfering with VEGF-A/VEGFR2 pathway. Oncogene 31(26): 3136-3147.

Maia, M., DeVriese, A., Janssens, T., Moons, M., Lories, R. J., Tavernier, J., & Conway, E. M. (2011): CD248 facilitates tumor growth via its cytoplasmic domain. BMC Cancer 11: 162.

Montagner, M., & Sahai, E. (2020): *In vitro* models of breast cancer metastatic dormancy. Frontiers in Cell and Developmental Biology 8: 37.

Naumov, G. N., Akslen, L. A., & Folkman, J. (2006): Role of angiogenesis in human tumor dormancy: animal models of the angiogenic switch. Cell Cycle 5(16): 1779-1787.

Neophytou, C. M., Kyriakou, T. C., & Papageorgis, P. (2019): Mechanisms of metastatic tumor dormancy and implications for cancer therapy. International Journal of Molecular Sciences 20(24): 6158.

Noy, P. J., Lodhia, P., Khan, K., Zhuang, X., Ward, D. G., Verissimo, A. R., Bacon, A., & Bicknell, R. (2015): Blocking CLEC14A-MMRN2 binding inhibits sprouting angiogenesis and tumour growth. Oncogene 34(47): 5821-5831.

Ohta, Y., Fujii, M., Takahashi, S., Takano, A., Nanki, K., Matano, M., Hanyu, H., Saito, M., Shimokawa, M., Nishikori, S., Hatano, Y., Ishii, R., Sawada, K., Machinaga, A., Ikeda, W., Imamura, T., & Sato, T. (2022): Cell-matrix interface regulates dormancy in human colon cancer stem cells. Nature n.pag.

Oki, T., Nishimura, K., Kitaura, J., Togami, K., Maehara, A., Izawa, K., Sakaue-Sawano, A., Niida, A., Miyano, S., Aburatani, H., Kiyonari, H., Miyawaki, A., & Kitamura, T. (2014): A novel cell-cycle-indicator, mVenus-p27K-, identifies quiescent cells and visualizes G0-G1 transition. Scientific Reports 4: 4012.

Opavsky, R., Haviernik, P., Jurkovicova, D., Garin, M. T., Copeland, N. G., Gilbert, D. J., Jenkins, N. A., Bies, J., Garfield, S., Pastorekova, S., Oue, A., & Wolff, L. (2001): Molecular characterization of the mouse Tem1/endosialin gene regulated by cell density *in vitro* and expressed in normal tissues *in vivo*. The Journal of Biological Chemistry 276(42): 38795-38807.

Osisami, M., & Keller, E. (2013): Mechanisms of metastatic tumor dormancy. Journal of Clinical Medicine 2(3): 136-150.

Páez, D., Labonte, M. J., Bohanes, P., Zhang, W., Benhanim, L., Ning, Y., Wakatsuki, T., Loupakis, F., & Lenz, H. J. (2012): Cancer dormancy: a model of early dissemination and late cancer recurrence. Clinical Cancer Research: An Official Journal of the American Association for Cancer Research 18(3): 645-653.

Park, J., Wysocki, R. W., Amoozgar, Z., Maiorino, L., Fein, M. R., Jorns, J., Schott, A. F., Kinugasa-Katayama, Y., Lee, Y., Won, N. H., Nakasone, E. S., Hearn, S. A., Küttner, V., Qiu, J., Almeida, A. S., Perurena, N., Kessenbrock, K., Goldberg, M. S., & Egeblad, M. (2016): Cancer cells induce metastasis-supporting neutrophil extracellular DNA traps. Science Translational Medicine 8(361): 361ra138.

Park, S. Y., & Nam, J. S. (2020): The force awakens: metastatic dormant cancer cells. Experimental & Molecular Medicine 52(4): 569-581.

Phan, T. G., & Croucher, P. I. (2020): The dormant cancer cell life cycle. Nature Reviews Cancer 20(7): 398-411.

Png, K. J., Halberg, N., Yoshida, M., & Tavazoie, S. F. (2011): A microRNA regulon that mediates endothelial recruitment and metastasis by cancer cells. Nature 481(7380): 190-194.

Recasens, A., & Munoz, L. (2019): Targeting Cancer Cell Dormancy. Trends in Pharmacological Sciences 40(2): 128-141.

Rettig, W. J., Garin-Chesatt, P., Healey, J. H., Su, S. L., Jaffe, E. A., & Oldt, L. J. (1992): Identification of endosialin, a cell surface glycoprotein of vascular endothelial cells in human cancer. Proceedings of the National Academy of Sciences of the United States of America 89(22): 10832-10836.

Risson, E., Nobre, A. R., Maguer-Satta, V., & Aguirre-Ghiso, J. A. (2020): The current paradigm and challenges ahead for the dormancy of disseminated tumor cells. Nature Cancer 1(7): 672-680.

Singh, A., Veeriah, V., Xi, P., Labella, R., Chen, J., Romeo, S. G., Ramasamy, S. K., & Kusumbe, A. P. (2019): Angiocrine signals regulate quiescence and therapy resistance in bone metastasis. JCI Insight 4(13): e125679.

Summers, M. A., McDonald, M. M., & Croucher, P. I. (2020): Cancer cell dormancy in metastasis. Cold Spring Harbor Perspectives in Medicine 10(4): a037556.

Teicher, B. A. (2019): CD248: A therapeutic target in cancer and fibrotic diseases. Oncotarget 10(9): 993-1009.

Tomkowicz, B., Rybinski, K., Sebeck, D., Sass, P., Nicolaides, N. C., Grasso, L., & Zhou, Y. (2010): Endosialin/TEM-1/CD248 regulates pericyte proliferation through PDGF receptor signaling. Cancer Biology & Therapy 9(11): 908-915.

Valastyan, S., & Weinberg, R. A. (2011): Tumor metastasis: molecular insights and evolving paradigms. Cell 147(2): 275-292.

Valdez, Y., Maia, M., & M. Conway, E. (2012): CD248: Reviewing its role in health and disease. Current Drug Targets 13(3): 432–439.

Wang, S., & Lin, S.-Y. (2013): Tumor dormancy: potential therapeutic target in tumor recurrence and metastasis prevention. Experimental Hematology & Oncology 2(1): 29.

Yadav, A. S., Pandey, P. R., Butti, R., Radharani, N. N. V., Roy, S., Bhalara, S. R., Gorain, M., Kundu, G. C., & Kumar, D. (2018): The Biology and therapeutic implications of tumor dormancy and reactivation. Frontiers in Oncology 8: 72.

Yeh, A. C., & Ramaswamy, S. (2015): Mechanisms of cancer cell dormancy – another hallmark of cancer?. Cancer Research 75(23): 5014-5022.

Zanivan, S., Maione, F., Hein, M. Y., Herná Ndez-Fernaud, J. R., Ostasiewicz, P., Giraudo, E., & Mann, M. (2013): SILAC-based proteomics of human primary endothelial cell morphogenesis unveils tumor angiogenic markers. Molecular & Cellular Proteomics 12(12): 3599-3611.

Zhang, B., Nguyen, L. X. T., Li, L., Zhao, D., Kumar, B., Wu, H., Lin, A., Pellicano, F., Hopcroft, L., Su, Y. L., Copland, M., Holyoake, T. L., Kuo, C. J., Bhatia, R., Snyder, D. S., Ali, H., Stein, A. S., Brewer, C., Wang, H., … Marcucci, G. (2018): Bone marrow niche trafficking of miR-126 controls the self-renewal of leukemia stem cells in chronic myelogenous leukemia. Nature Medicine 24(4): 450-462.

Creative Biolabs, Recombinant antibody (2022) https://www.creativebiolabs.net/ontuxizumab-overview.htm (pristupljeno 2.2.2022.)

8. CURRICULUM VITAE

I was born on August 26, 1997 in Rijeka, Croatia. I attended primary school "Osnovna škola Vladimir Gortan" in Rijeka, graduating in 2012. as a student of generation. Afterwards, I attended general gymnasium programme at the secondary school "Prva sušačka hrvatska gimnazija" in Rijeka, graduating in 2016. and was among a few selected students to receive recognition for educational achievements. During my secondary education, I participated at the International Summer School of Science in Požega, Croatia in 2015. and attended Biology state competition organized by Croatian Ministry of Science and Education in 2016. After graduation, I enrolled in an undergraduate (2016.-2019.) and graduate programme in Molecular Biology (2019.-2022.) at the Faculty of Science, University of Zagreb, Zagreb, Croatia. I completed my undergraduate studies with *Summa cum laude*. Throughout my studies, I was a recipient of multiple scholarships, including STEM Scholarship and Scholarship "City of Rijeka", and was awarded Rector's award for team scientific research paper in 2020. Additionally, I volunteered at the science popularization events "Night of biology" (2017.-2019.) and "BioStudoLogija" (2018.), organized by the Faculty of Science. During 2021., I enrolled in an Erasmus+ programme, working as an intern at the Department of Pharmacology at the Max Planck Institute for Heart and Lung Research, Bad Nauheim, Germany for six months, under the supervision of Prof. Dr. Stefan Offermanns. During my stay there, I was working on multiple research projects involving tumor dormancy and metastasis, including my master's thesis research, and was supervising undergraduate students during their laboratory skill practice internship.

9. SUPPLEMENTARY MATERIAL

Supplementary material include vector structures and inserted sequences used in experiments.

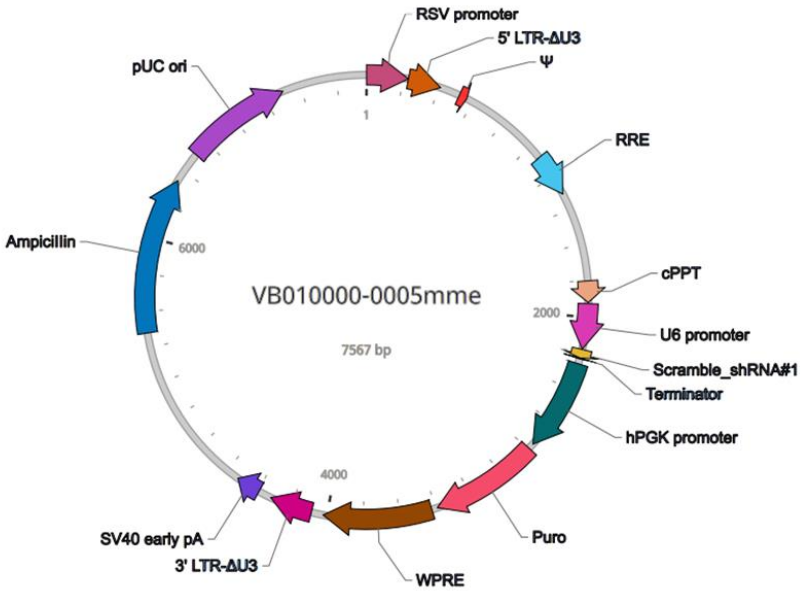

Supplementary figure 1. Mammalian shRNA Knockdown Lentiviral Vector with inserted *scramble shRNA* used in lentiviral transduction experiment (Figure obtained from VectorBuilder).

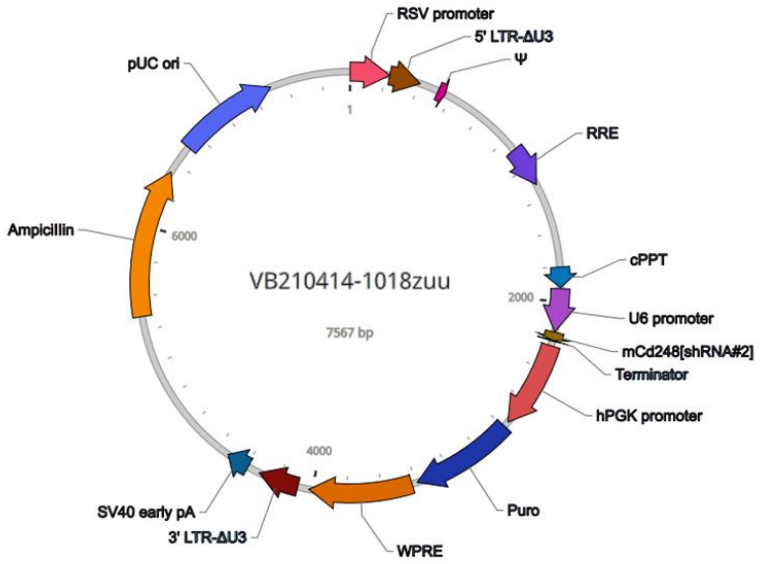

Supplementary figure 2. Mammalian shRNA Knockdown Lentiviral Vector with inserted *mouse CD248 (TEM1)* used in lentiviral transduction experiment (Figure obtained from VectorBuilder).

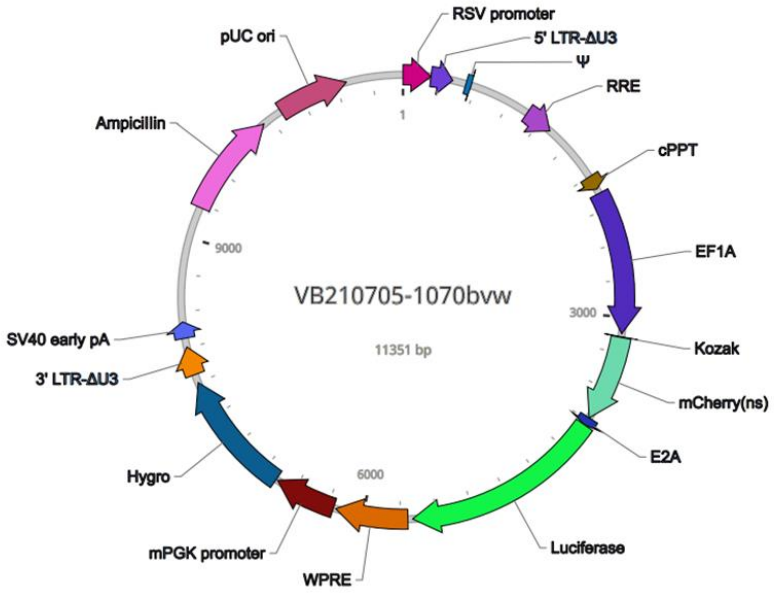

Supplementary figure 3. Mammalian Gene Expression Lentiviral Vector with inserted *EF1A promoter* and *mCherry* and *Luciferase ORF* used in lentiviral transduction experiment (Figure obtained from VectorBuilder).

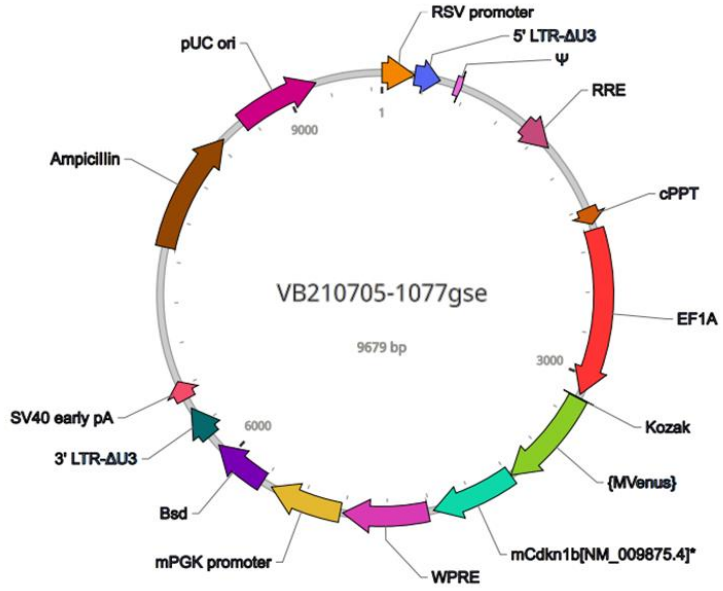

Supplementary figure 4. Mammalian Gene Expression Lentiviral Vector with inserted *EF1A promoter* and *mVenus-mouse Cdkn1b (p27K^{-}) ORF* used in lentiviral transduction experiment (Figure obtained from VectorBuilder).

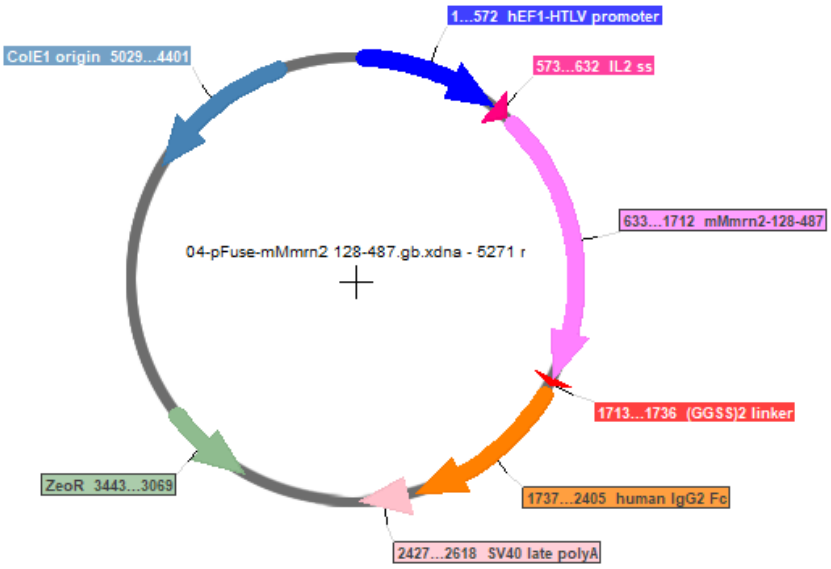

Supplementary figure 5. Plasmid vector containing human IgG2 Fc designed for the construction of Fc-fusion proteins with inserted *MMRN2*$^{(128-487)}$ used in recombinant protein expression and concentration experiment (Figure obtained from Serial Cloner V2.5).

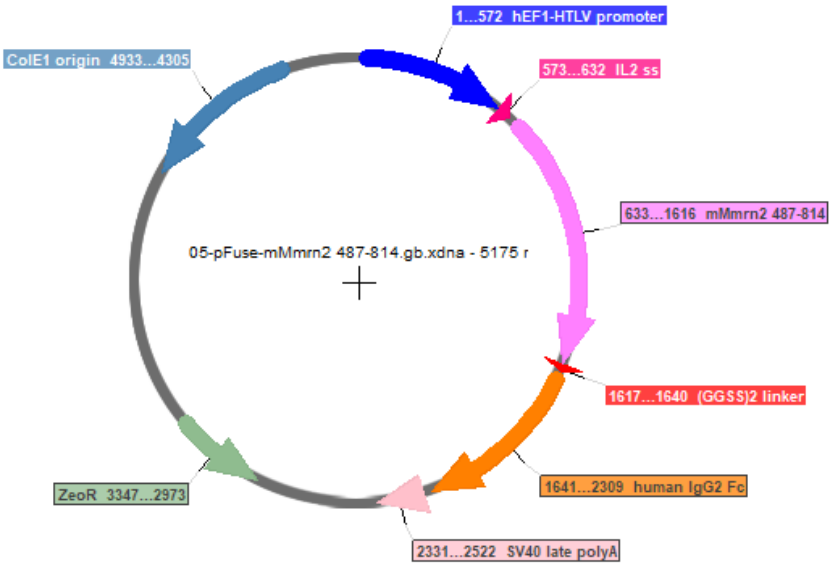

Supplementary figure 6. Plasmid vector containing human IgG2 Fc designed for the construction of Fc-fusion proteins with inserted *MMRN2*$^{(487-814)}$ used in recombinant protein expression and concentration experiment (Figure obtained from Serial Cloner V2.5).